

A new method of determining the inclination angle in interacting binaries

Tariq Shahbaz

University of Oxford, Department of Physics, Nuclear Physics Laboratory, Keble Road, Oxford, OX1 3RH, UK

8 August 2018

ABSTRACT

We describe a method of determining the system parameters in non-eclipsing interacting binaries. We find that the extent to which an observer sees the shape of the Roche-lobe of the secondary star governs the amount of distortion of the absorption line profiles. The width and degree of asymmetry of the phase-resolved absorption line profiles show a characteristic shape, which depends primarily on the binary inclination and gravity darkening exponent. We show that, in principle, by obtaining high spectral and time resolution spectra of quiescent cataclysmic variables or low mass X-ray binaries in which the mass-losing star is visible, fitting the shape of absorption line profiles will allow one to determine not only the mass function of the binary, but also the binary inclination and hence the mass of the binary components.

Key words: binaries: – close – stars: fundamental parameters

1 INTRODUCTION

The determination of the binary inclination in non-eclipsing interacting binaries has been problematic for many years. One method widely used to determine the binary inclination in dwarf novae and the soft X-ray transients is to measure the ellipsoidal variations of the late-type star (Warner 1995; van Paradijs & McClintock 1995). These variations are caused by the companion star presenting differing aspects of its distortion to the observer, giving rise to a double-humped modulation whose amplitude is strongly dependent on the binary inclination. However, one problem in measuring the ellipsoidal variations of the secondary star is that the accretion disc can contribute a significant amount of flux at optical wavelengths (e.g. typically about 10–50 per cent in the soft X-ray transients). This contribution must be accounted for if the binary inclination is to be determined using optical light curves (see Charles 1996 and references within).

Here we describe a technique which uses the information available about the shape of the Roche-lobe of the secondary star, and its effect on the shape of the absorption line profiles. The parameters we measure are insensitive to the disc contribution, but dependent on the binary inclination and gravity darkening exponent. We will first give a brief description of the model and then describe the effect of the mass ratio, inclination, limb and gravity darkening on the shape of the line profiles. Finally, we will simulate data and proceed to fit it using the model.

2 THE MODEL

2.1 Basic assumptions

We model a binary system where the primary is a compact object and the secondary a “normal” star. The basic assumption is that the secondary star fills its Roche-lobe, and that its rotation is synchronised with the orbital motion. A grid consisting of a series of quadrilaterals is set up over the surface of the secondary star, accounting for the tidally distorted shape in the 3-body potential of two stellar cores (i.e taking the gravitational potential of each star to be like that of a point mass). The equation for the Roche potential is solved numerically. Then, for each element the radial velocity and visibility throughout the orbital cycle are computed (see van Paradijs & McClintock 1995). After taking into account the intrinsic line profile, assumed to be a Gaussian function, the predicted rotation profile at each orbital phase is obtained by summing the line intensities of all the surface elements. This yields the phase-resolved rotation profile of the secondary star. The model parameters which govern the shape of the line profiles are the binary mass ratio q ($=M_1/M_2$ where M_1 and M_2 are the masses of the compact object and secondary star respectively), the inclination i , the mean effective temperature T_{eff} the mean gravity, $\log g$, of the secondary star, and ff , the filling fraction of the Roche lobe defined as the ratio of the secondary star radius to the inner Lagrangian point distance, both being measured along the line of centres of the two stars.

The Roche lobe filling secondary star in our model is not a normal star, it is distorted. In the model, we assume that the absorption line arises from a surface of constant optical depth and that that surface coincides with the Roche lobe equipotential. Because of gravity darkening, the two surfaces do not exactly coincide, but for simplicity we shall take the approximation that they do. This may introduce some uncertainty in the specific intensity distribution over the secondary star, since integrating over an equipotential will select different parts of the absorption spectrum. We can estimate the validity of this assumption by determining the scale height in the secondary star that gives rise to the absorption line spectrum (i.e. the stellar reversing layers), and the effect this has on the observed surface. For late-type main sequence stars in a 10 hr binary this turns out to be 0.03 per cent of the stellar radius (Allen 1973). Such an atmosphere will have the following effect. If we assume that the secondary fills its critical Roche potential at Ω_{crit} then the observed surface level will be located at $\Omega_{crit} - \delta\Omega$. For a late-type star (K5V) in a 10 hr binary, the observed surface lies at a potential corresponding to a star that fills 99.97 per cent of its Roche lobe ($\delta\Omega$ is 0.03 per cent of the stellar radius; i.e. the stellar reversing layers for a K5V star; see Allen 1973). Using the model we calculate that there is less than a 1 per cent change in the shape of the absorption line profiles for a star that fills its Roche lobe compared to when it underfills it by 0.03 percent. Note however, that in general $\delta\Omega$ depends on position on the surface, as the opacity of the stellar material is dependent on the local temperature and gravity (Tjemkes, Zuiderwijk & van Paradijs 1986).

2.2 The intensity distribution

The distribution of the specific intensity over the stellar surface is determined by a linear limb darkening law and the flux by von Zeipel's gravity darkening law (von Zeipel 1924). The latter states that the radiation flux at any point of the stellar surface is proportional to the local acceleration of gravity. The exponent of this law depends on the structure of the secondary star. It can be either 0.08 for a star with a convective envelope (Lucy 1967) or 0.25 for a star with a radiative envelope. Therefore, using Stefan's law one can obtain the local temperature of each element of area. The local surface gravity can be obtained by computing the derivatives of the local gravitational potential. Given the mean effective temperature of the secondary star, the effective temperature of each element is calculated such that the integrated luminosity over the stellar surface is given by the observed luminosity, which is fixed by the mean effective temperature. Similarly, the local gravity is calculated such that the integrated gravity over the surface of the star is given by the mean gravity of the secondary star.

In order to determine the rotation profile, we first need to determine the temperature and gravity of each surface element and then use model atmospheres to determine the appropriate local specific intensity. The line intensity is then integrated over all the visible surface elements to give the phase-resolved rotation profile. We compute model spectra of the Ca I absorption line at 8446 Å for a wide range of effective temperatures and gravities. We use this line as an example since it is present in K-type stars, is isolated and clear from telluric features and is strongly dependent on temperature and gravity. From these spectra we then compute the line intensity which we store in a temperature-gravity grid. The line intensity at a given temperature and gravity on the secondary star can then be interpolated from this grid. For the limb darkening at each surface element we use a linear limb darkening law, the coefficients of which are interpolated from the values given in Al-Naimiy (1978). However, it should be noted that the limb darkening coefficient refers to the continuum and is different for the absorption line (see section 3.4 and Collins & Truax 1995). Since the line value is unknown for late-type stars, we use the continuum value.

3 MODEL SIMULATIONS

In order to show the effects of different model parameters on the shape of the absorption lines arising from the secondary star, we compute the rotation profiles and then convolve them with a Gaussian function, representing the resolution of a spectrograph. Ideally one would determine the actual response function of the spectrograph by looking at the arc calibration spectra and then use it to broaden the rotation profiles. In most cases the response function is Gaussian. In each test case we assume an instrumental resolution of 6 km s⁻¹ (FWHM); the intrinsic line width is assumed to be negligible (less than the velocity dispersion of the model profile, 2 km s⁻¹; which is similar to the turbulence velocity in late-type main sequence stars; Gray 1992). Hence the effective line shape is only due to the combined effects of Doppler broadening and the finite instrumental resolution, since the pixel size is comparable to the intrinsic line width. Throughout the simulations we will assume a secondary star with $T_{eff}=4500$ K and $\log g=4.5$, corresponding to a K5V star. We will also assume the the observed radial velocity semi-amplitude K_2 is fixed at 162 km s⁻¹ ($K_2=v_2 \sin i$ where v_2 is the true velocity of the secondary star).

Fig. 1 shows phase-resolved trailed spectra for three values of β (0.0, 0.08 and 0.16) using $q=2.0$ and $i=60^\circ$. These parameters give an expected mean rotational broadening $V_{rot} \sin i$ of 78 km s⁻¹. The absorption line profiles are in the rest frame of the secondary star. As one can see, the line profiles change shape with orbital phase, becoming strongly asymmetric near phase 0.5 (see Fig. 5). We measure two quantities from the model profiles, the full width at half maximum (FWHM) and the degree of asymmetry (DOA) of the line profiles (see Robertson 1986 for a full description). Note that the choice for the method used to estimate the degree of asymmetry is purely arbitrary, and only serves as a means of comparison. The degree of asymmetry is a dimensionless parameter varying between -100 and 100. A degree of asymmetry of zero corresponds to a symmetric profile, whereas a triangle having one vertical side would have a degree of asymmetry of ± 8.1 (its sign depending on which side is the vertical one). In all the models produced in this paper the DOA is in the range -2 to 2.

There are a number of simple tests that one can use to estimate the numerical uncertainty in the model. For a system at zero inclination there will be no observed radial velocity of the secondary star. The observer will see the same projected

surface of the secondary star all the time. Also there should be no rotational broadening of the absorption lines. Using $K_2=0.0$ km s⁻¹ and $\beta=0.08$ for a Roche lobe filling star we find that the DOA and FWHM are independent of orbital phase. The DOA is 0.0 and the FWHM of the line profile is within less than 0.1 km s⁻¹ of the instrumental broadening. We obtain the same results by setting $i=0^\circ$. One also expects for a spherical star that the FWHM and degree of asymmetry of the absorption lines should be constant and independent of orbital phase and inclination. We can simulate a spherical star by severely underfilling the lobe of the secondary star (i.e. using $ff=0.1$). Doing this, we find for a given set of system parameters, the FWHM of the lines are constant to within 0.5 km s⁻¹ and the DOA of the lines are within 0.1 of zero; both the FWHM and DOA of the lines are independent of orbital phase and binary inclination.

In Fig. 2 we show the general effects of limb (u) and gravity darkening for a system at $i=50^\circ$. The case where the limb darkening (u) is zero and the temperature distribution across the secondary star is constant ($\beta=0.0$), describes the effect of the physical shape of the Roche-lobe. Using $\beta=0.08$ changes the shape of the FWHM curves, whereas using full limb darkening changes the mean value. It should be noted that the radial velocity semi-amplitude ($K_2 = v_2 \sin i$) depends on the true velocity of the secondary star (v_2) and the binary inclination. Since v_2 only sets the absolute velocity scale of the system, in subsequent sections we will assume the observable parameter K_2 to be fixed, so that we can also compare the FWHM of the line profiles for different model parameters. Below we describe in detail the effects of the various model parameters on the shape of the line profiles.

3.1 The effects of inclination

We find that for a given gravity darkening exponent, the shape of the FWHM curves, especially near phase 0.4, are dependent on the binary inclination. At low inclinations the observer generally sees the same surface elements on the star, and so the FWHM light curves will be almost symmetric around phase 0.25. The largest value for the FWHM of the line profiles will be for the profiles at phase 0.25, since at this phase the observer sees the full length of the distorted star, with the largest range of velocities. As the binary inclination increases, the shape of the light curve changes. The general shape of the light curve up to phase 0.25 is the same, however, after phase 0.25 the profiles start to change significantly because the observer starts to see a larger fraction of the inner distorted face of the star. This results in the line profiles becoming highly asymmetric because of the heavy limb and gravity darkening associated with the surface elements on the inner face of the star. Fig. 3 shows the FWHM and DOA curves for fixed values of $\beta=0.00$ and $\beta=0.08$ with $i=20^\circ$, 40° and 60° . As the binary inclination increases, the degree of asymmetry of the line profiles near phase 0.45 shifts to more negative values. In Fig. 3c we show in detail the effects of the binary inclination on the DOA of the line profiles, for low binary inclinations $i=0^\circ$, 2° , 4° , 8° , 15° using $\beta=0.08$. The asymmetry near phases 0.05 and 0.45 first shifts to more positive values as the inclination decreases. At the maximum DOA value, at $i \sim 15^\circ$, the DOA of the profile at all orbital phases then moves towards zero; at $i = 0.0^\circ$ the DOA of the phase resolved line profile are zero. From Fig. 3a and 3b it can also be seen that the minimum of the FWHM curves at phase 0.5 shifts towards phase 0.4. This shift of the minimum of the FWHM curves can be explained in terms of the observer seeing a larger fraction of the distorted inner face of the secondary star. Note that the degree of asymmetry of the line profiles near phase 0.25 is almost independent of the binary inclination. This is simply because the observer sees the full extent of the Roche lobe, which is almost the same for all inclination angles.

3.2 The effects of gravity darkening

As mentioned earlier the temperature distribution across the secondary star is governed primarily by the gravity darkening exponent. If $\beta=0.0$ then each surface element will emit the same flux. However, the inclination, line of sight effects and the shape of the Roche-lobe then govern the final flux distribution one observes. If β is large, then the surface elements with the least gravity, i.e. around the inner Lagrangian point, will be heavily gravity darkened. Even the surface elements near the spherical face are gravity darkened. These elements will have much lower temperatures than the elements near the pole of the star and thus will emit less flux. This implies that the cores of the line profiles at phases 0.0 and 0.5 will appear to be filled by a small amount, since these cool elements of area have low velocities. Fig. 4 shows the temperature distribution along the line of centres of the two stars, for $\beta=0.0$, 0.08 and 0.16 .

The effects of gravity darkening can be seen in Fig. 1. Here we show the profiles for $\beta=0.0$, $\beta=0.08$ and $\beta=0.16$. As one can see, the asymmetry in the profiles near phase 0.45 changes dramatically. Fig. 5 shows the FWHM and DOA curves for a system at $i=20^\circ$ and $i=60^\circ$ with $\beta=0.00$, 0.08 and 0.16 . As the gravity darkening exponent increases, the degree of asymmetry of the line profiles near phase 0.45 shifts to more negative values. For high inclination systems the minimum of the FWHM curves at phase 0.5 shifts towards phase 0.4 (a similar effect to that observed by increasing the binary inclination).

3.3 The effects of the mass ratio

Fig. 6 shows a system with $i=60^\circ$, $\beta=0.08$ and $q=1$ (stars), 5 (circles) and 10 (crosses). The main effect q has is to change the FWHM of the line profiles; the FWHM changes fastest with q for small values of q . The DOA of the profiles do not change much. q governs the amount of distortion and hence the shape of the Roche-lobe. However, the rate of change of the distortion is greatest at low values of q . In Fig. 7 we measure the amount of distortion by computing the ratio of the Cartesian coordinates x/y , x/z and z/y at the surface of the secondary star, where x is defined to lie along the line joining the centre

of mass of the two stars, y to lie in the orbital plane and z perpendicular to the orbital plane, i.e along the axis of rotation. In fact, at extreme values of q , the amount of distortion of the secondary star tends towards a constant value, which explains the apparent convergence of the FWHM curves at large q .

3.4 The effects of limb darkening

In the model, we use values for the limb darkening coefficient which refer to the continuum (Al-Naimiy 1978), since the actual value, which varies in the absorption line, is unknown for late-type stars. We assume a local intrinsic line broadening due to turbulence of 2 km s^{-1} (i.e. the velocity dispersion of the data), which corresponds to a change in wavelength of $\sim 0.04\text{\AA}$. For a given temperature we find that the continuum limb darkening coefficient varies by less than 0.01 per cent (from the wavelength dependence of the limb darkening coefficient; Al-Naimiy 1978) in the intrinsic absorption line profile. The effect of this change is negligible compared to the change in the limb darkening coefficient (~ 15 per cent) as a result of the temperature variations across the star.

The effects of limb darkening on the mean value for the rotational broadening of the secondary star have been noted before. Welsh, Horne & Gomer (1995) find that the mean broadening changes by up to 14 percent, between zero and full limb darkening. Here we explore the effects of the actual value used for the local limb-darkening coefficient (for each element on the surface of the star) and how its value changes the shape of the line profiles, in particular the shape of the FWHM curves. Fig. 8 shows the effect of zero ($u=0.0$) and full ($u=1.0$) limb darkening on the shape of the FWHM curves, for $i=30^\circ$ and $i=50^\circ$ with fixed $\beta=0.08$. The FWHM curves have been normalised to the value at phase 0.25. Note that the whole shape of the FWHM curves changes between full and zero limb darkening, especially near phase 0.0 and 0.5.

4 THE EFFECT OF ZONAL FLOWS AND STAR-SPOTS

4.1 Zonal flows

Rapid rotation, strong tidal force and non-uniform heating are present in all interacting binaries. These effects give rise to circulation currents within the atmospheres of the mass losing stars. The results of Martin & Davey (1995) suggests that for temperature rise of 1000K the predicted flows are comparatively slow (less than 1 km s^{-1}). One would expect such low velocities, since the sound speed of material in the outer layers of the star is $\sim 7 \text{ km s}^{-1}$ (Frank, King & Raine 1992). We have simulated such flows by adding a random velocity between 0 and 1 km s^{-1} to the radial velocity of the elements on the surface of the star. The observed profile is determined as before (see section 2.1). We find that although the shapes of the line profiles do change, the general trends in the FWHM and DOA curves are very similar to the simulations for a star without the zonal flows (see Fig. 9). Therefore we conclude that the effects due to the gravity darkening and inclination are dominant. However, it should be noted that we have assumed a random velocity flow pattern; the exact 3-D velocity pattern is probably very complicated, but if we use a flow pattern that is restricted around the equator of the star, the result does not change.

4.2 Star-spots

In CVs tidal dissipation is likely to produce uniform rotation as well as synchronous rotation. Atmospheric motions have been used to explain the anomalous brightness distribution on the surface (a hot-spot near the inner Lagrangian point) on some of the irradiated secondary stars in cataclysmic variables (Davey & Smith 1992). The simulations of Martin & Davey (1995) show hot buoyant material rising at phase 0.4 and sinking near phase 0.9 and phase 0.0. They then go on to suggest that the converging flow at the back of the star may gather up magnetic field lines and so produce a magnetic star-spot (dark-spot).

In order to estimate the effects of hot- and dark-spots on the asymmetry of the line profiles, we simulated absorption line profiles for a star with a dark-spot centred at the back side of the star and a hot-spot centred at the inner Lagrangian point. Martin (1988) showed that the position of the white dwarf and bright spot on the accretion disc in cataclysmic variables would give rise to irradiation that was not too far from being symmetric about the inner Lagrangian point. Therefore we describe the spot as a circle extending to a latitude R_{spot}° away from its centre (i.e. the inner Lagrangian point for the hot-spot and the back-side of the star for the dark-spot). The effective temperature in the dark-spot region is lower than it would have been in the absence of the spot by 750 K. This is the typical observed temperature difference in RS CVn systems and T Tauri stars (Rodono 1986). We have used a hot spot which has an temperature increase of 1000 K, but note that this is an extreme case. For dwarf novae or soft X-ray transients in quiescence the temperature increase at the inner face of the secondary is probably much less. We have used spot sizes of 10 degrees.

Fig. 10 shows FWHM and DOA curves using $i=60^\circ$ and $\beta=0.08$ and spot sizes of 10 degrees, for a star with a dark- and hot-spot and with no spots. As one can see, only the dark-spot has an appreciable effect on the shape of the line profiles near phase 0.05. However, its effect depends on its size. It should be noted that the simulations shown here are an extreme case; no dark-spot at the back side of the secondary star has been observed in any CV.

5 SIMULATING DATA

In this section we describe the method we use to determine the system parameters from simulated data. We determine the binary inclination, the gravity darkening exponent and also the fraction of light arising from the secondary star.

In order to simulate data, we computed 21 rotation profiles using $i=60^\circ$, $\beta=0.08$, $q=2.0$, $K_2=162 \text{ km s}^{-1}$ and $T_{eff}=4500 \text{ K}$ at orbital phases between 0.0 and 0.5. We also allowed for the effects of a velocity flow across the star (see section 4.1). We then convolved these functions with a template star spectrum (a K5 V star) and then added Gaussian distributed noise. The observed template star spectrum was taken using the Utrecht Echelle Spectrograph (FWHM=6 km s⁻¹). The effects of an accretion disc were simulated by veiling the observed flux by 33 per cent.

To estimate the typical signal-to-noise we might expect to achieve for each spectrum, we use the dwarf nova AE Aqr as an example. Observing this object with the high resolution spectrograph attached to the Keck telescope for 6 mins would give a signal-to-noise ratio of about 80 per pixel (using the program HIRES with V=12 mags at 6500 Å). In practice, the absorption line features will be smeared by an amount $2\pi K_2 t \cos(2\pi\phi)/P$, due to the orbital motion of the secondary star during the length of each exposure (t) at orbital phase ϕ . This effect is included by convolving the phase resolved broadened template star spectra with a rectangular function with the appropriate velocity width. In this example the effect of smearing is about 10 km s^{-1} , i.e. $t \sim 0.01P$. The final phase resolved simulated data have a velocity dispersion of 2 km s^{-1} . The spectra were then Doppler shifted into the rest frame of the secondary star.

It should be noted that in simulating data we first applied the instrumental broadening to the absorption line spectrum and then convolved it with the rotation profile of the secondary star. However, in reality the absorption line spectrum is first broadened by the rotation of the secondary star and then by the response of the instrument. Using Gaussian and Lorentz instrumental response functions and a highly asymmetric rotation profile (i.e. one at phase 0.45) we performed the convolutions in the orders described above. We find that the maximum difference in the convolved profiles is less than 0.02 per cent. It will clearly be hidden in the noise of the simulated data. This small difference is due to the fact that the instrumental broadening is more than a factor of 10 less than the rotational broadening of the secondary star.

5.1 Measuring $V_{rot} \sin i$

Tidal synchronisation will make the angular velocity of the secondary star constant. Since the star is distorted, the linear rotational velocity will vary with longitude around the star and the true $V_{rot} \sin i$ will vary with orbital phase. Many authors have attempted to measure the changes in the phase resolved rotational broadening in cataclysmic variables (Welsh, Horne & Gomer 1995; Casares et al. 1996). In particular Casares et al. (1996) determined it in AE Aqr. They compare the $V_{rot} \sin i$ variations with the FWHM of model line profiles. However, it should be noted that there are many systematic errors in the procedure they use. The method to extract $V_{rot} \sin i$ is flawed, i.e. using the Gray profile (Gray 1992) to broaden a template star spectrum which is then compared with the data, because the secondary star is non-spherical. In this section, we calculate the systematic effects introduced by only fitting the $V_{rot} \sin i$ variations with the FWHM curves. Note that if one wants to determine the binary inclination then one has to fit the actual shape of the absorption lines using a model that predicts the correct broadening function for a star that fills its Roche-lobe.

First, we extract the $V_{rot} \sin i$ variations from the simulated data. Note that the specific intensity versus temperature and gravity relations we use in the simulated data are for the total intensity in the spectral range 6380–6460 Å. We broadened the template star spectrum from 90 to 100 km s⁻¹ in steps of 2 km s⁻¹ using the Gray rotation profile (Gray 1992). A linear limb-darkening coefficient of 0.65 was used (Al-Naimiy 1978). We then performed an optimal subtraction between the phase resolved broadened template and data spectra. The optimal subtraction routine subtracts a constant times the template spectrum from the data, adjusting the constant to minimize the residual scatter between the spectra. The scatter is measured by carrying out the subtraction and then computing the χ^2 between this and a smoothed version of itself. The constant, f , represents the fraction of light arising from the template spectrum, i.e. the secondary star. The optimal values of $V_{rot} \sin i$ and f are obtained by minimising the χ^2 . Note that the data point at phase 0.475 (Fig. 11) has a larger velocity width (FWHM) than its neighbours. This is because, at this phase, the line profile is highly asymmetric (see section 3), and so the method of using the Gray profile fails badly. The next step is to determine the model FWHM line profile variations. We do this by determining the rotation profile for a given set of model parameters, i.e. inclination and gravity darkening exponent. We then convolve this with a Gaussian function representing the instrumental resolution. The FWHMs of the phase dependent line profiles are then measured.

The measured phase resolved values of $V_{rot} \sin i$ are then fitted with the FWHM variations of the line profiles. We exclude the data point at phase 0.475, since it is clearly incorrect. This allows us to perform a grid search in the $\beta - i$ plane, allowing confidence levels to be determined. We obtain a best fit at $i=42^\circ$ and $\beta=0.14$. Fig. 11 shows the measured phase resolved $V_{rot} \sin i$ variations and the best model fit. In Fig 12 we show the 68 and 90 per cent confidence levels of the fits in the $\beta - i$ plane. As one can see, even at the 90 per cent confidence level, we do not recover the original system parameters of the simulated data. There seems to be a systematic shift towards lower values for the inclination and larger values for the gravity darkening exponent. This result is not so surprising if we consider the fact that we are only using the widths of the lines. One can see from the model simulation in section 3, that at certain orbital phases, i.e. 0.1 and 0.4, the widths of the line profiles may be the same, but the actual shapes of the profiles are not. One has to fit the actual shape of the absorption lines using a model that predicts the correct broadening function for a star that fills its Roche-lobe.

5.2 Fitting the line profiles

In principle, one would like to use many absorption lines in the fitting procedure. However, the advantages of using single line profiles can be seen by comparing the normalised line intensity of the Ca I line with the total specific intensity in the spectral range 6380–6460 Å (see Fig. 13). Generally, using a wide spectral range will tend to include absorption lines that are not so sensitive to temperature and gravity. The net effect will be to decrease the sensitivity of the fitting procedure. Fitting many strongly temperature and gravity dependent single lines will make the fitting procedure more sensitive. In this section we show that we can recover the binary inclination by only fitting a single line.

In order to fit the phase resolved simulated spectra, we first determine a rotation profile for a given set of model parameters, i.e. orbital phase, inclination and gravity darkening exponent, which we then convolve with the template star spectrum (i.e. the isolated Ca I line). Note that the template star spectrum has already been broadened by the finite resolution of the spectrograph (6 km s^{-1}), so we do not have to allow for this in the model. We then perform an optimal subtraction between the phase resolved broadened template and data spectra. The values of χ^2 for each orbital phase are then summed up. This allows us to perform a grid search in the $\beta - i$ plane, allowing confidence levels to be determined. We obtained the best fit at $i=66^\circ$ and $\beta=0.06$.

We have also simulated data with a signal-to-noise ratio of 80 per spectrum, as previously, but now with a 10 degree hot- and dark-spot placed at the inner Lagrangian point and the back side of the secondary star respectively, and a random velocity flow pattern (see section 4) over the star. We find that it only changes the inclination solutions by 8 degrees; the $1-\sigma$ uncertainty in the model fit is 12 degrees. Therefore within the uncertainties the star-spots and zonal flows do not have a significant effect on the inclination angle determined.

In the data simulation we have assumed the instrumental response to be a Gaussian function; for most spectrographs this assumption is good. However, in order to see the effects of fitting data taken with a spectrograph that does not have a Gaussian instrumental response, we simulated data using a skewed Gaussian function as the instrumental response. The function is a normal Gaussian, except that we multiply the FWHM of half the curve by $(\sinh \gamma / (1 - \exp -\gamma))$. This means that one side of the curve is the same as a Gaussian with that FWHM, and the other side is skewed. In this case we used $\gamma=2.0$; using $\gamma=0.0$ would give a Gaussian profile. We then went on to fit the data, using a model with a Gaussian function as the instrumental response, and find that it only changes the inclination solutions by at most 3 degrees.

It should also be noted that we have used continuum limb-darkening coefficients in the model. The absorption lines in late-type stars will have core limb-darkening coefficients much less than the value appropriate for the continuum; the precise value requires detailed calculations (Collins & Truax 1995). However, in order to estimate the uncertainties in over-estimating the limb-darkening in the line we simulated data using limb-darkening coefficients which were 10 percent of the appropriate continuum value. We then proceeded to fit the data using the model described. We find that using the model in which the limb-darkening coefficients is the appropriate continuum value, the $1-\sigma$ uncertainty in the inclination angle solution is 15 degrees, the best fit is at $i=66^\circ$. Using the model in which the limb-darkening coefficients is 10 percent of the continuum value, the $1-\sigma$ inclination solutions are 4 degrees higher, β is 0.02 higher. Therefore, despite using a model in which we over-estimate the limb-darkening coefficient in the absorption line, we can still determine the binary inclination.

If we assume that we can fit 16 single line profiles that have similar intensity versus temperature and gravity relations to those for the Ca I line, then our uncertainties are reduced by a factor 4. In Fig. 14 we show the 68 per cent confidence level of the fits using 16 lines in the $\beta - i$ plane. The cross marks the best fit and the star marks the true parameters of the simulated data. For $\beta=0.08$, we find $i=50^\circ-68^\circ$ (68 per cent confidence). In Fig. 15 we show the phase resolved values of χ^2_ν and the veiling factor (f , the fraction of light arising from the secondary star) obtained using the best fit model. As one can see, we have demonstrated that by fitting a single line profile, one can at least recover the binary inclination. It should be noted that the accuracy with which we can determine the inclination is dependent on the signal-to-noise of the phase resolved spectra. In this example it is 80 in a single observation. This can easily be increased by observing the binary system for two orbital cycles and then coadding the spectra on half the orbital period, since the spectra between phases 0.5 and 1.0 will be symmetric to those between phase 0.0 and 0.5. This will increase the signal-to-noise of each individual spectrum by a factor 2. Also note that simultaneously fitting many single lines that are correlated with temperature and gravity in different ways may allow one to also extract the gravity darkening exponent. However, this involves a detailed examination of model line profiles in order to select single lines which have different temperature and gravity relations. This will be the subject of a future paper.

6 DISCUSSION AND CONCLUSIONS

By obtaining high spectral and time resolution spectra of cataclysmic variables or low mass X-ray binaries, systems in which the absorption features of the secondary star can be seen, one can perform a radial velocity study of the secondary star and also determine the binary mass ratio (see Marsh, Robinson & Wood 1994 for a full description of this kind of study). However, as pointed out in this paper, it is also possible to extract the binary inclination by fitting the absorption lines profiles of the secondary star.

Some of the assumptions inherent in the model which predicts the shape of the line profiles should be noted. The main assumption in the model is that the observed surface of constant optical depth coincides with the Roche potential surface. However, we find that this only changes the shape of the line profiles by less than 1 per cent. Zonal flow patterns and/or

dark- hot-spots can have an appreciable effect on the shape of the line profiles. However, the extent of these effects depends very much on the magnitude of the zonal flows and the size of the spots. Simulations show that only very low velocities are predicted for zonal flows (Martin & Davey 1995).

The characteristic modulations in the width of the line profiles are, in principle, similar to the ellipsoidal modulations, which are due to the observer seeing differing aspects of the gravitationally distorted secondary star as it orbits a compact object. However, this method uses the velocity information across the star as well as the projected area. It should also be noted that unlike modelling the ellipsoidal variations in the optical, where the accretion disc contribution must be taken into account, this method is independent of the disc contribution (as long as the disc contribution is not such that it totally swamps the secondary star features). This implies all emission and continuum sources, i.e. from a bright spot or a gas stream, will only affect the determination of the veiling factor and not the shape of the absorption lines. However, care must be taken in choosing the lines to use for this kind of analysis; the lines must be clear of any weak emission features arising from the disc or accretion flow.

The determination of the binary inclination is essential if one wants to obtain the mass of the binary components in non-eclipsing binaries. The method described here can be applied to bright cataclysmic variable stars or low mass X-ray binaries, in which one can resolve the absorption lines of the secondary star, and where the amount of X-ray heating is small. The effect of heating implies that one cannot use temperature sensitive absorption lines such as the Na I 8183-8184 Å doublet in the modelling (see Friend et al. 1990 and references within for the effects of irradiation). Such systems are the dwarf novae and the soft X-ray transients. This method allows one to determine all the system parameters from a high spectral resolution (few km s⁻¹) spectroscopic study.

We have described a method of determining the binary inclination in non-eclipsing interacting binaries by fitting the shape of the absorption lines arising from the secondary star. We find that the amount of distortion of the absorption line profiles is primarily due to the extent to which an observer sees the shape of the Roche-lobe of the secondary star. We show that, in principle, by obtaining high spectral and time resolution spectra of quiescent dwarf novae or the soft X-ray transients, where the disc is low, fitting the shape of absorption line profiles will allow one to determine the binary inclination. Our simulations show that previous efforts to determine the inclination are flawed, and give systematically lower values for the inclination.

ACKNOWLEDGEMENTS

I would like to thank Bill Welsh and Phil Charles for valuable discussions, and Barry Smalley for computing the model atmospheres. I also thank the referee R.C. Smith for his careful reading and criticism of the paper that has undoubtedly enhanced its content. This work was carried out on the Oxford Starlink node using the ARK software package to plot the figures.

REFERENCES

- Allen C.W., 1973, *Astrophysical Quantities*, The Athlone Press, pg 213
 Al-Naimiy H.M., 1978, *Ap&SS*, 53, 181
 Casares J., Mouchet M., Martinez-Pais I.G., Harlaftis E.T., 1996, *MNRAS*, 282, 182
 Charles P.A., 1996, in *Compact Stars in Binaries*, eds J.van Paradijs, E.P.J.van den Heuvel, E.Kuulkers, IAU Symp 165, 341
 Collins II G.W., Truax R.J., 1995, *ApJ*, 439, 860
 Davey S.C., Smith R.C., 1992, *MNRAS*, 257, 476
 Frank J., King A.R., Raine D.J., 1992; *Accretion Power in Astrophysics*, Cambridge University Press, p 13
 Friend M.T., Martin J.S., Smith R.C., Jones D.H.P., 1990, *MNRAS*, 246, 654
 Gray D.F., 1992, *The Observations and Analysis of Stellar Photospheres*, Wiley-Interscience, New York
 Lucy L.B., 1967, *ZfAp*, 65, 89
 Marsh T.R., Robinson E.L., Wood J.H., 1994, *MNRAS*, 266, 137
 Martin J.S., 1988, DPhil Thesis, University of Sussex
 Martin T.J., Davey S.C., 1995, *MNRAS*, 275, 31
 Robertson J.G., 1986, *PASP*, 98, 1220
 Tjemkes S.A., Zuiderwijk E.J., van Paradijs J., 1986, *A&A*, 154, 77
 van Paradijs J., McClintock J.E., 1995 in *X-ray Binaries*, eds Lewin W.H.G., van Paradijs J., van den Heuvel E.P.J., Cambridge University Press, p 58
 von Zeipel H., 1924, *MNRAS*, 84, 665
 Welsh W.F., Horne K., Gomer R., 1995, *MNRAS*, 275, 649

FIGURE CAPTIONS

Figure 1: From left to right, the panels show the trailed absorption line profiles using $\beta=0.0, 0.08$ and 0.16 . For all the models $q=2.0, i=60^\circ$ and $K_2=162$ km s⁻¹. As one can see the width and the degree of asymmetry of the line profiles are dependent

on orbital phase and the value for β .

Figure 2: The general effects of limb and gravity darkening on the FWHM and DOA curves for a system at $i=50^\circ$. The case for $u=0.0$, $\beta=0.00$ (plus signs); $u=1.0$, $\beta=0.00$ (stars); $u=0.0$, $\beta=0.08$ (circles); $u=0.0$, $\beta=0.08$ (triangles) are shown. The gravity darkening changes the shape of FWHM curves whereas the limb darkening changes the mean value. The horizontal dashed line indicates where the degree of asymmetry of the line is zero.

Figure 3: The effects of inclination. 3(a) The FWHM and DOA curves for $\beta=0.00$. Models for $i=20^\circ$ (stars), 40° (circles) and 60° (crosses) are shown. The horizontal dashed line indicates where the degree of asymmetry of the line is zero. 3(b) Same as above but using $\beta=0.08$. 3 (c) The DOA curves for low binary inclinations, 0° , 2° , 4° , 8° , 15° , 30° and 60° , using $\beta=0.08$. As the binary inclination decreases the degree of asymmetry of the line profiles near phases 0.05 and 0.45 shifts to more positive values, then, at $i \sim 15^\circ$ the DOA of the line profiles moves towards zero. At $i = 0^\circ$ the DOA of all the phase resolved profiles are zero.

Figure 4: The temperature distribution on the surface of the secondary star along the line of centres of the binary components for $\beta=0.0$ (dotted line), 0.08 (solid line) and 0.16 (dashed lines). The distribution has been normalised to a mean temperature of 4500 K. As β increases the temperature of the elements of area near the inner Lagrangian point (L_1) also decreases. Thus these elements will emit less flux compared to regions near the pole of the secondary star.

Figure 5: The effects of gravity darkening. 5(a) The FWHM and DOA curves for fixed $i=20^\circ$. Models for $\beta=0.00$ (stars), 0.08 (circles), and 0.16 (crosses) are shown; 5(b) Same as above but with fixed $i=60^\circ$. As one can see the shape of the curves depends on the value for the binary inclination.

Figure 6: The effects of the binary mass ratio on the FWHM and asymmetry of the line profiles for fixed $i=60^\circ$. The curves are for $q = M_1/M_2=1$ (stars), 5 (circles) and 10 (crosses). The largest changes occur at small values of q . The horizontal dashed line indicates where the degree of asymmetry of the line is zero.

Figure 7: The distortion of the secondary star measured by computing the ratio of the Cartesian coordinates x/y , x/z and z/y at the surface of the secondary star x is defined to lie along the line joining the centre of mass of the two stars, y to lie in the orbital plane and z perpendicular to the orbital plane.

Figure 8: The effects of limb darkening. (a) The normalised FWHM and DOA curves for fixed $i=30^\circ$. Models for zero ($u=0.0$; crosses) and full ($u=1.0$; circles) limb darkening are shown; (b) Same as above but with fixed $i=50^\circ$.

Figure 9: (a) Same as Fig 3b but using zonal velocity pattern across the secondary star. (b) Same as Fig 5b but using a zonal velocity pattern across the secondary star. The curves are very similar to those without the velocity pattern because the actual velocities are very small (see Martin & Davey 1995).

Figure 10: The effects of star-spots (dark and hot-spot 10 degrees in radius; see section 4.2) on the FWHM and DOA curves for a system with $i=60^\circ$ and $\beta=0.08$. Also shown for comparison is the case with (zonal flow) and without (normal) a zonal velocity flow.

Figure 11: The $V_{rot} \sin i$ variations with orbital phase for the simulated data, obtained by optimally subtracting a template star broadened using the Gray (1992) profile from the phase resolved data. Also shown is the best fit obtained using the FWHM variations of the model line profiles (see section 4.1).

Figure 12: Results from fitting the $V_{rot} \sin i$ variations using the FWHM of the model line profiles. The 68 (dashed line) and 90 (solid line) percent confidence solutions are shown in the $\beta - i$ plane. The best model fit is marked at $i=42^\circ$ and $\beta=0.14$ (cross) and the true solution of the simulated data is also marked at $i=60^\circ$ and $\beta=0.08$ (star).

Figure 13: The normalised specific intensity as a function of temperature ($\log g=4.5$) in the Ca I 6439 Å absorption line compared to the total specific intensity in the spectral range 6380–6460 Å. As one can see the single line has a much stronger dependence on temperature and so is more sensitive to the fitting procedure outlined in section 5.2.

Figure 14: Results for fitting the Ca I line profile with the model described in section 3. The 68 percent confidence solution is shown in the $\beta - i$ plane. The best model fit is marked $i=66^\circ$ and $\beta=0.06$ (cross) and the true solution is also marked at $i=60^\circ$ and $\beta=0.08$ (star).

Figure 15: The results for the optimal subtraction of the simulated data and the best fit model. The top panel shows the χ^2_ν for each phase resolved spectrum. The bottom panel shows the fraction of light arising from the secondary star determined by the phase resolved optimal subtraction.

Figure 1

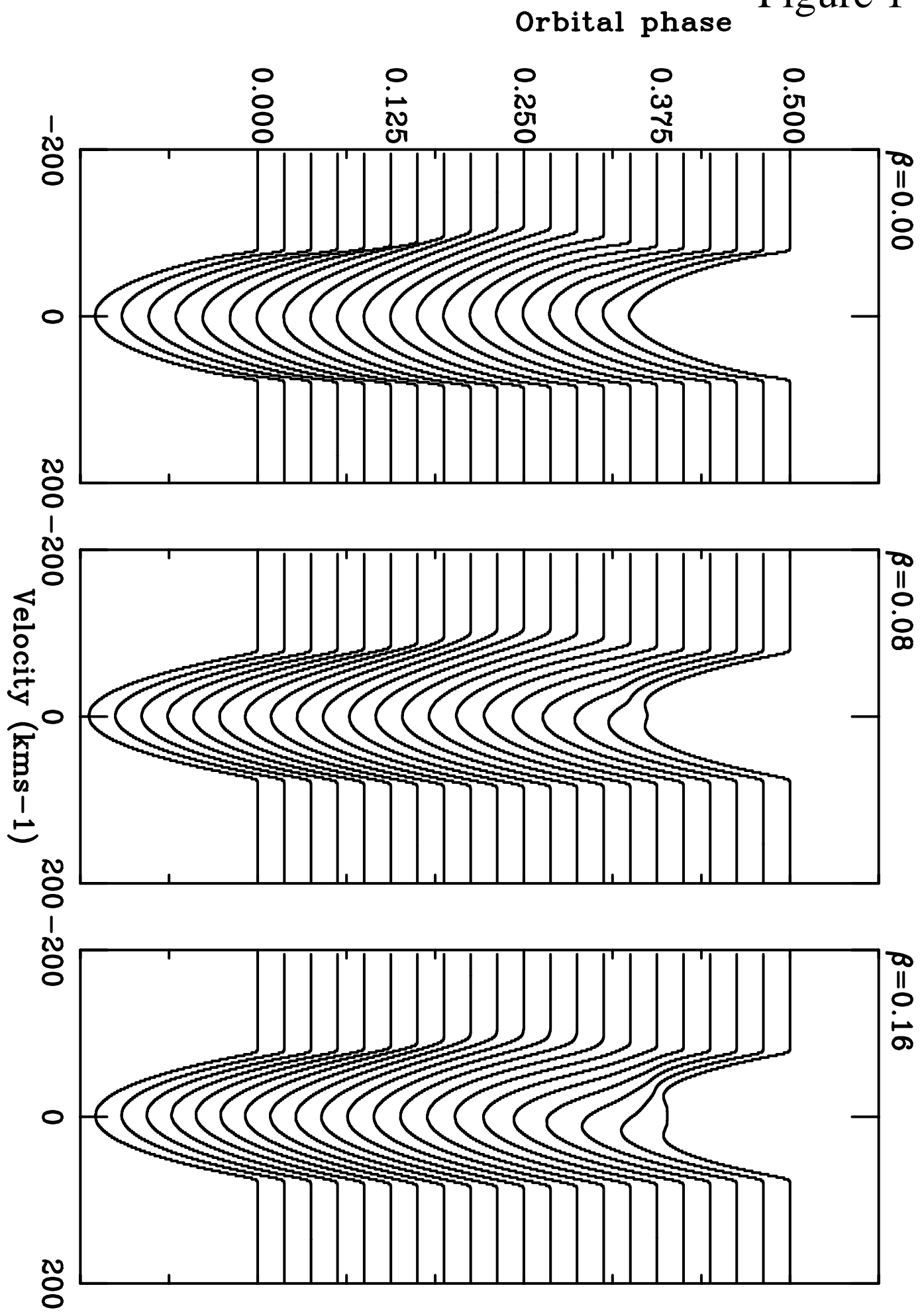


Figure 2

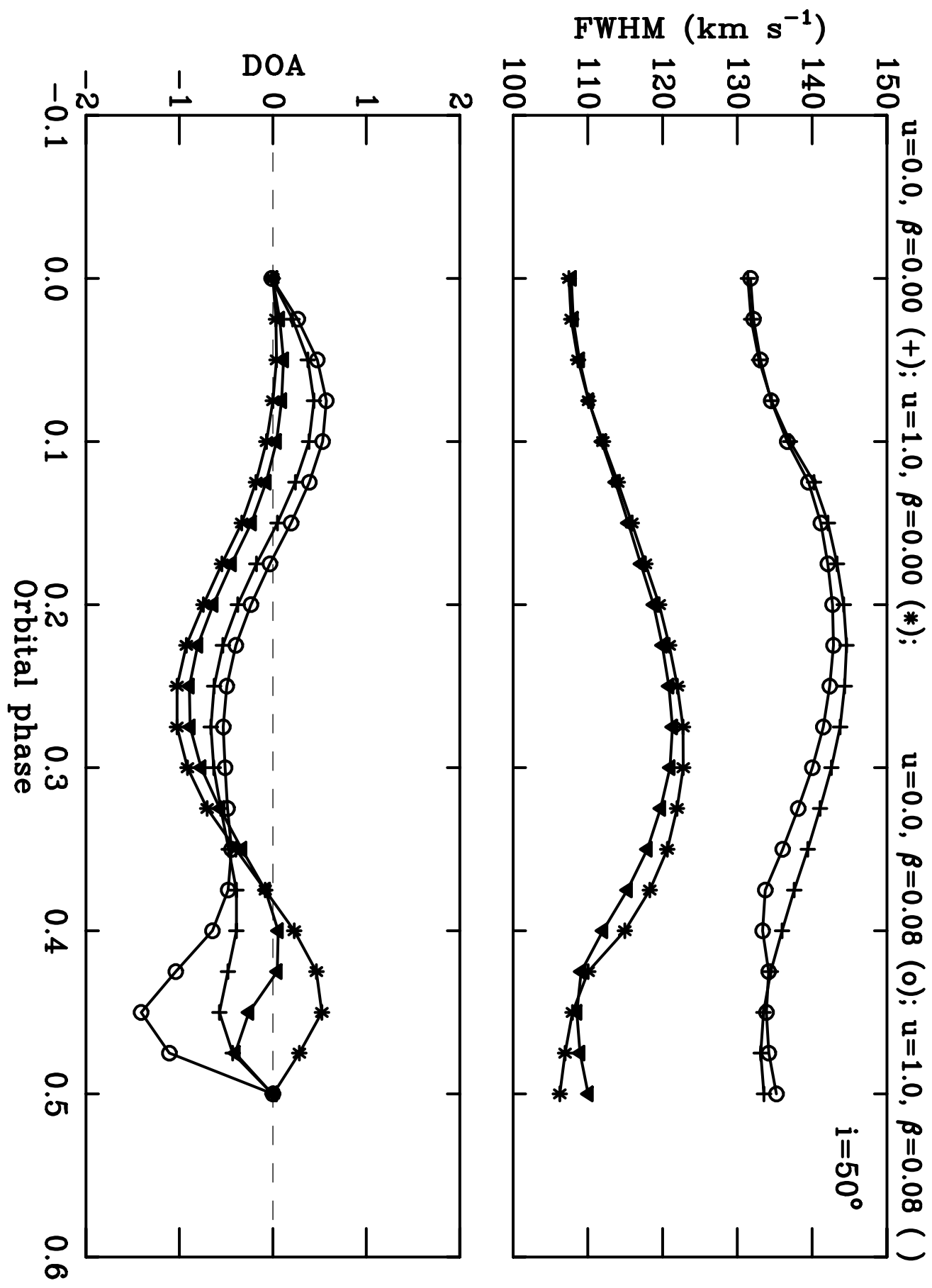


Figure 3a

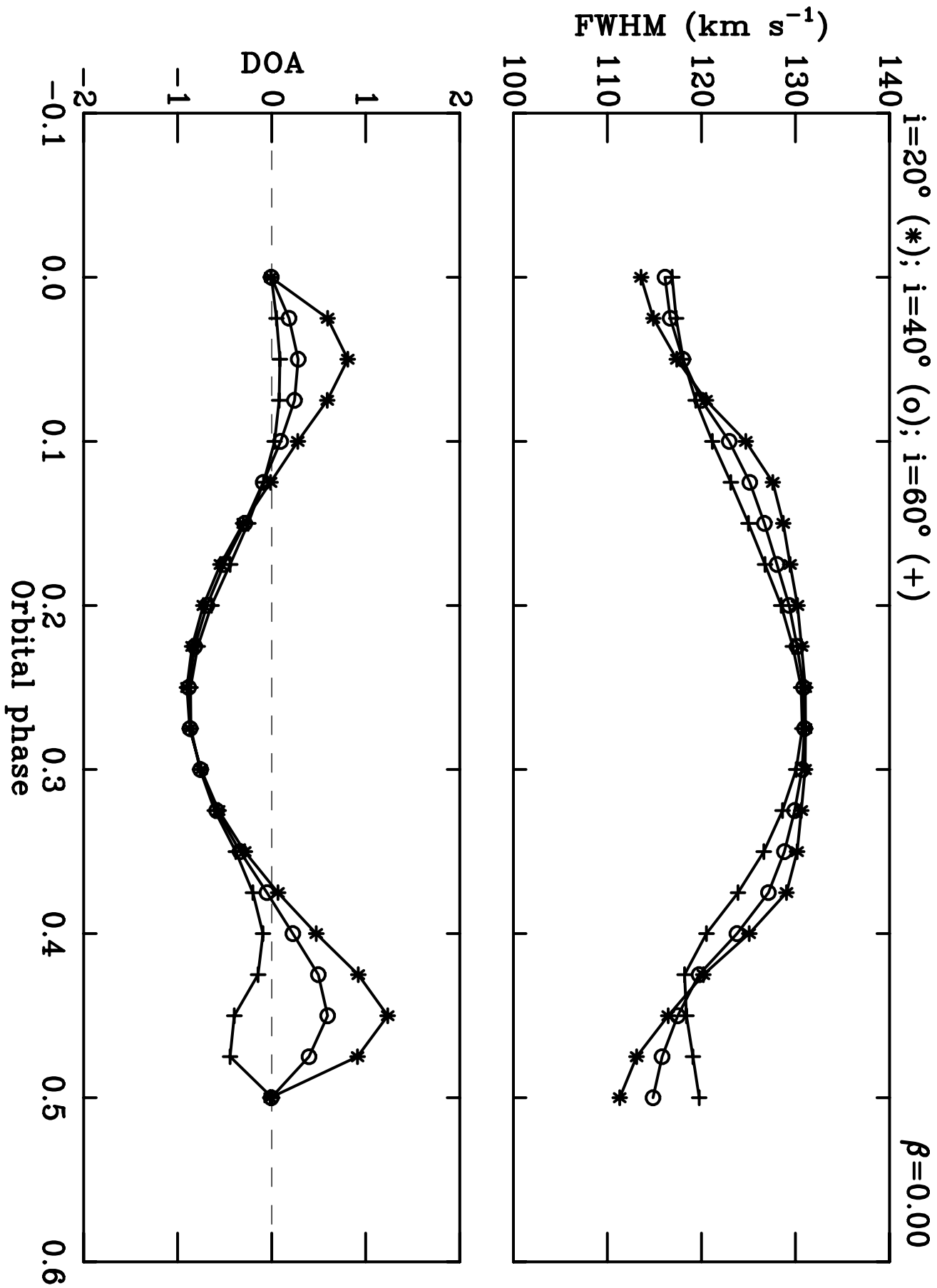


Figure 3b

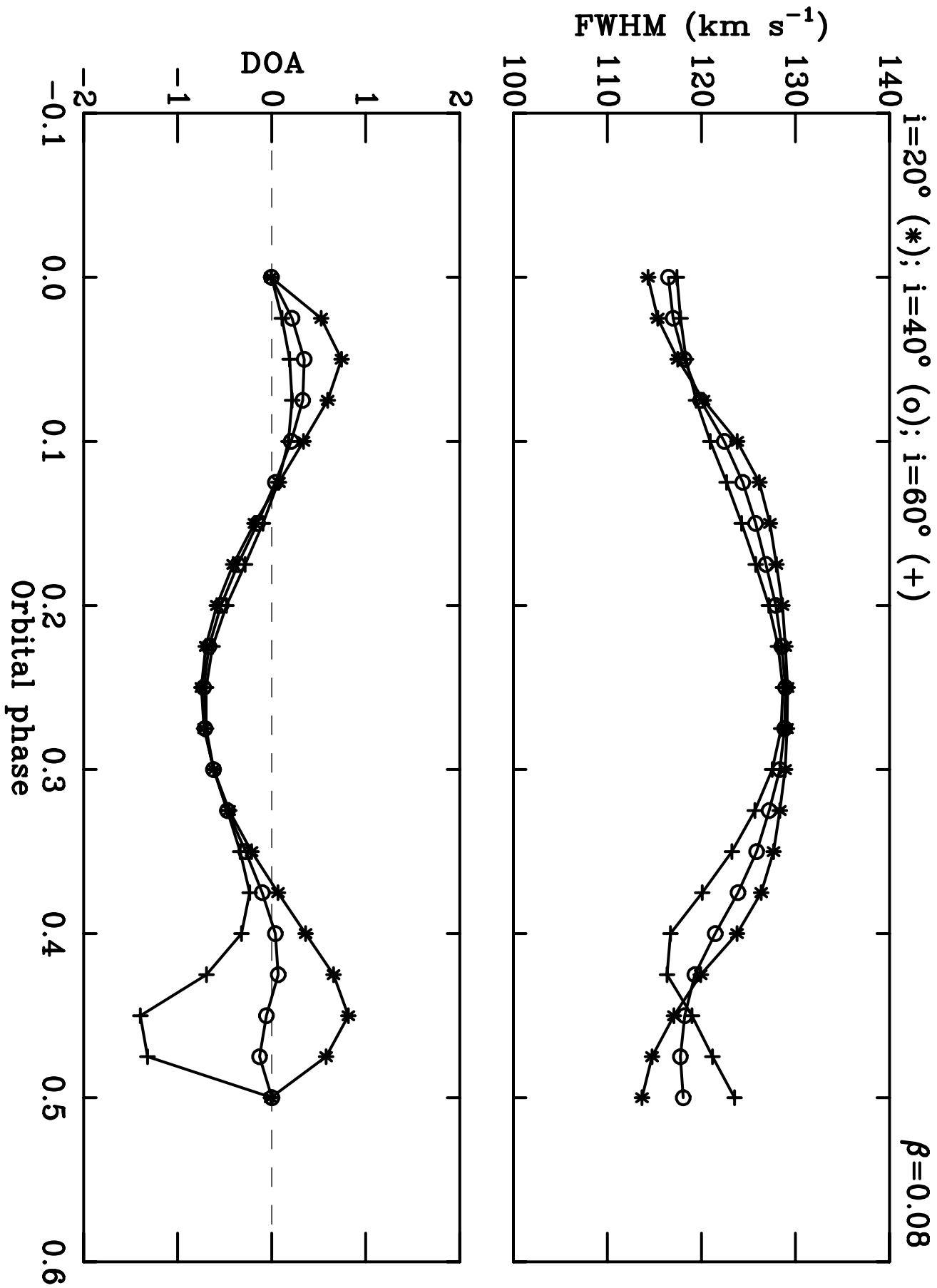


Figure 3C

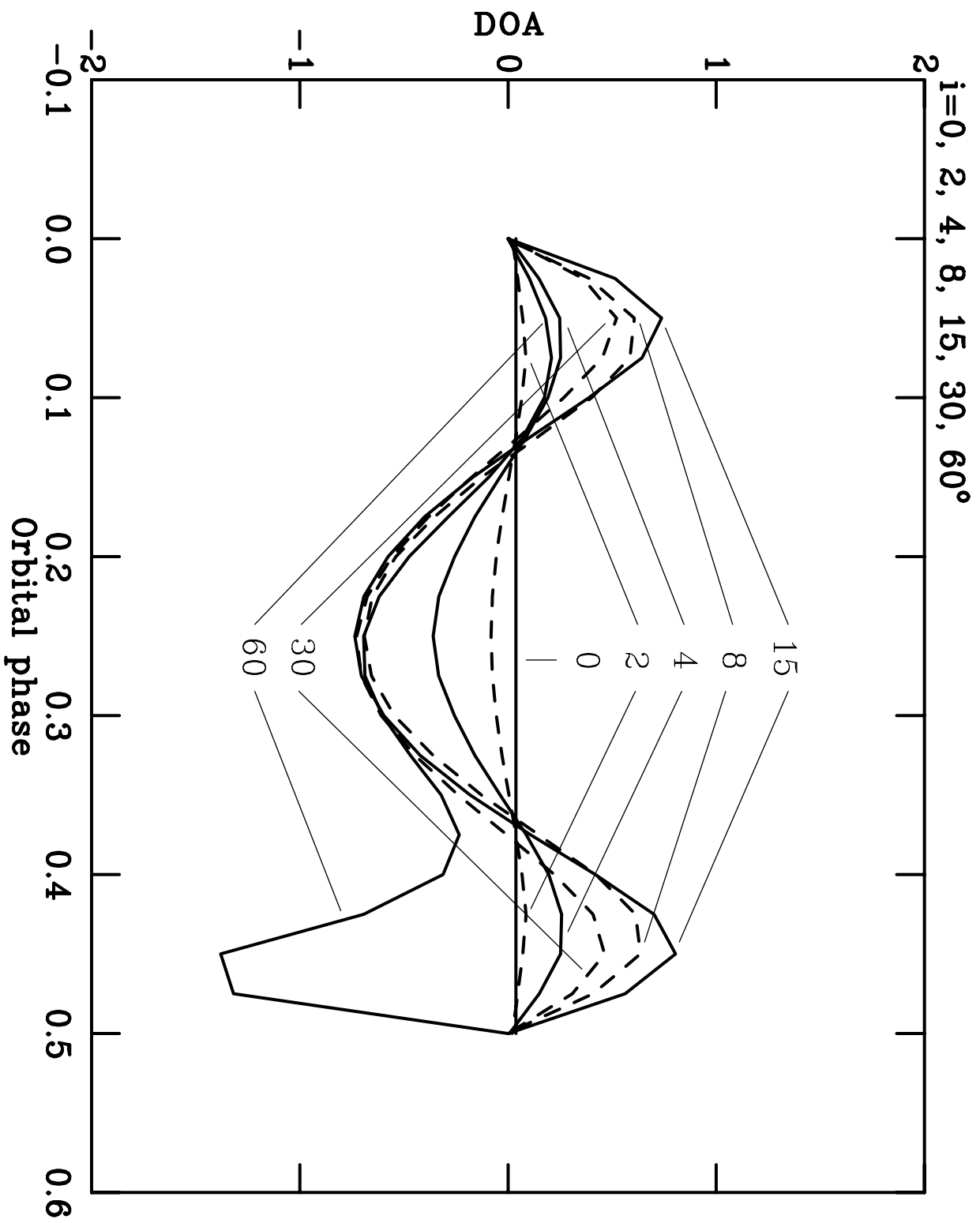


Figure 4

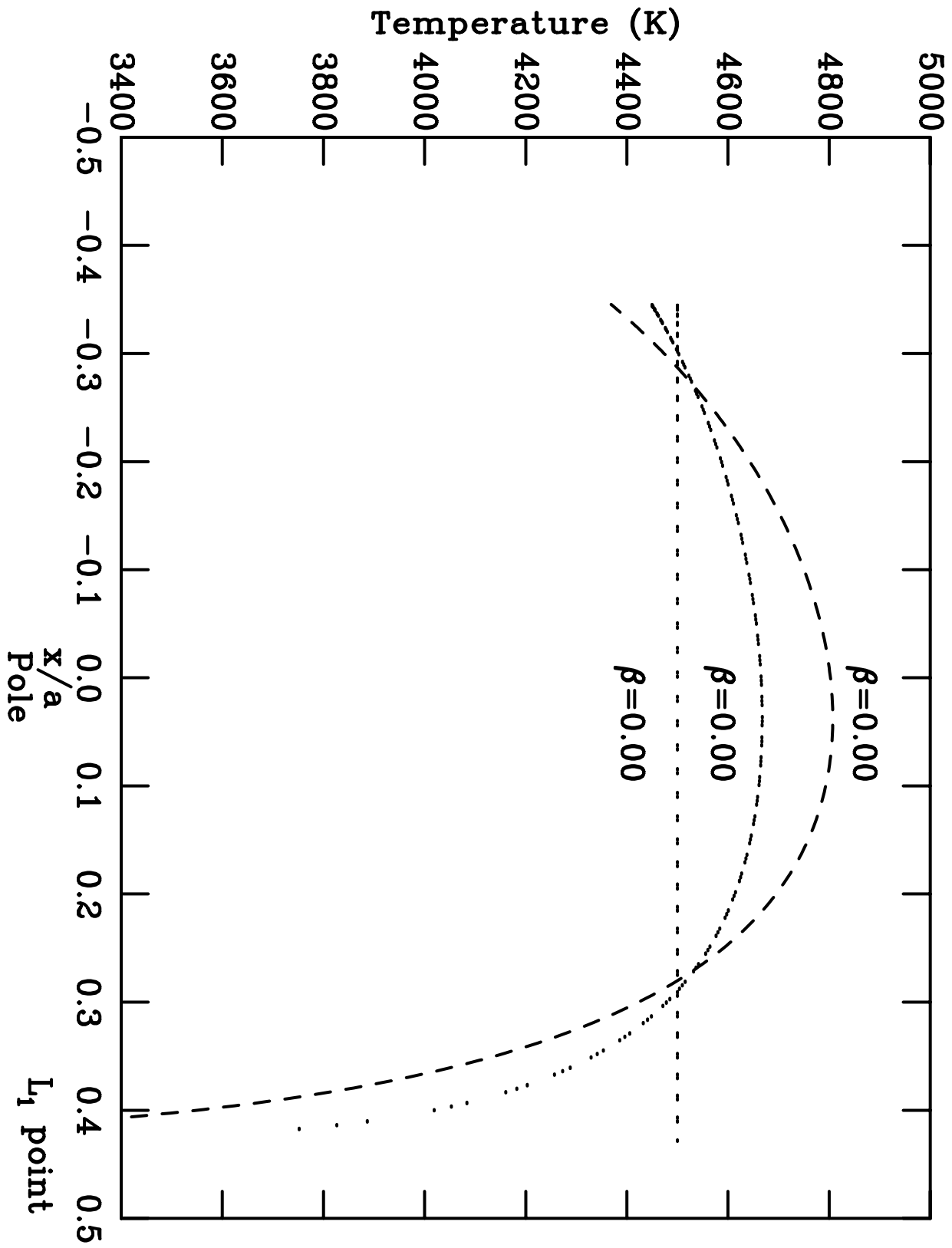


Figure 5a

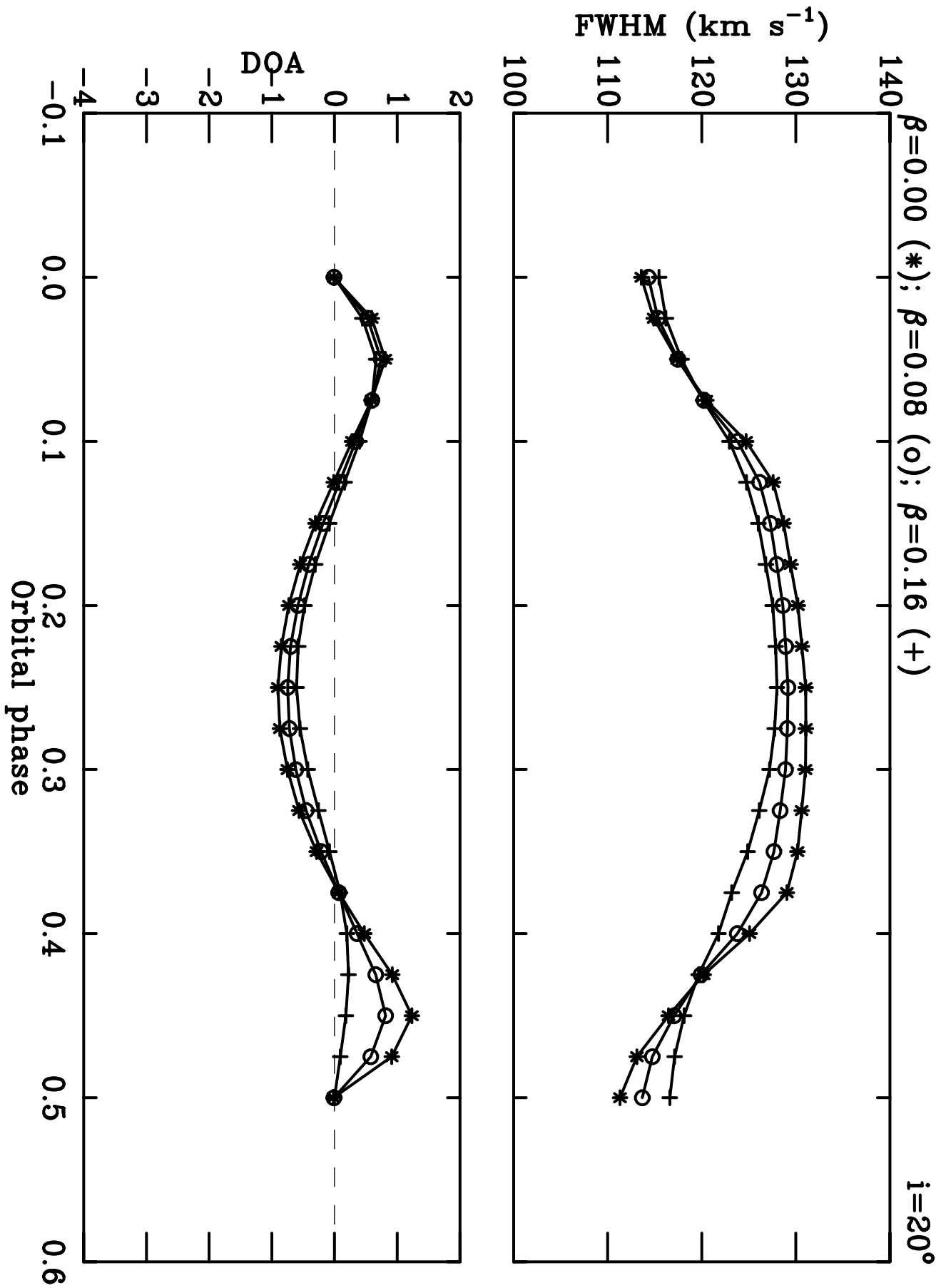


Figure 5b

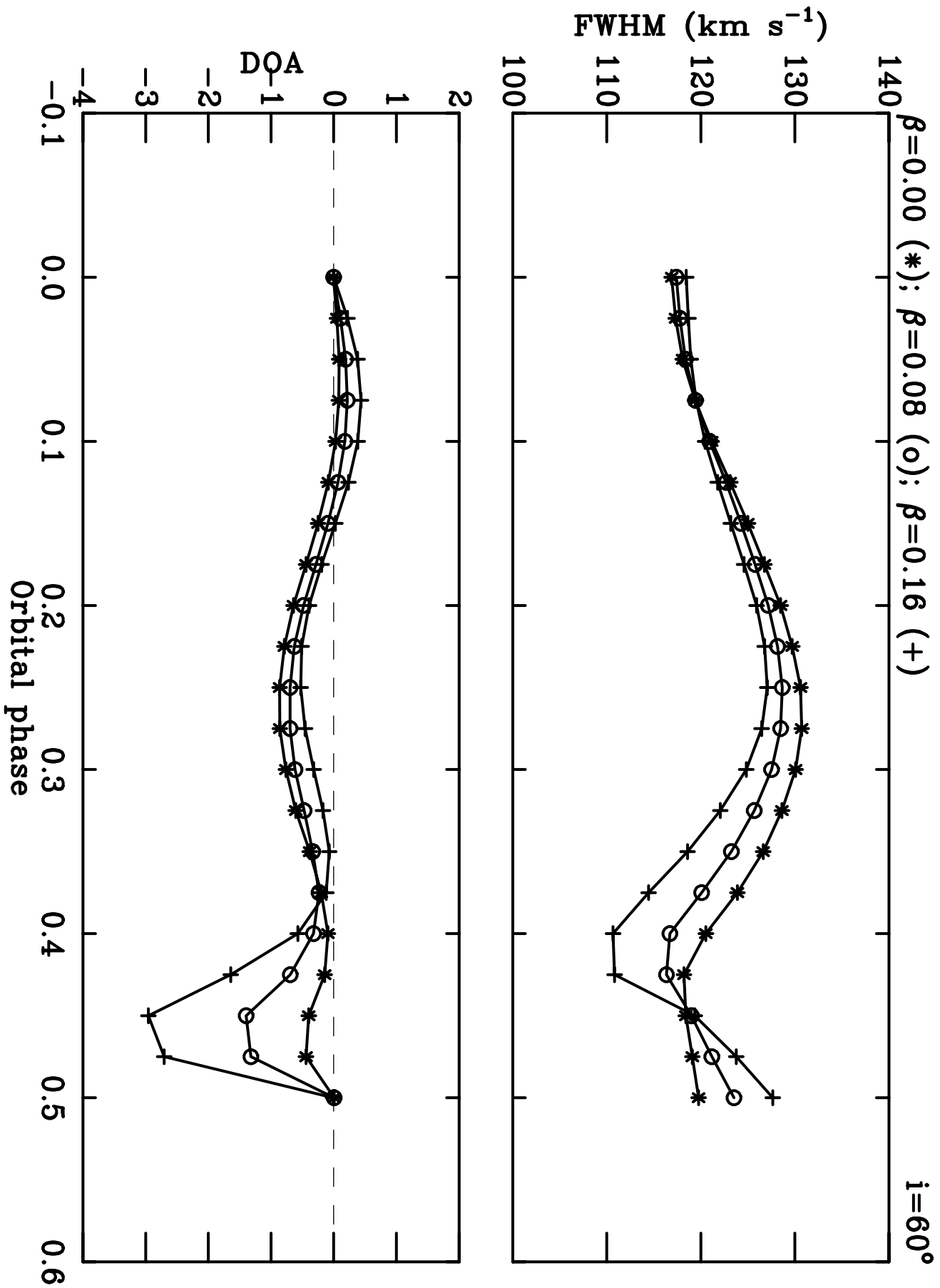


Figure 6

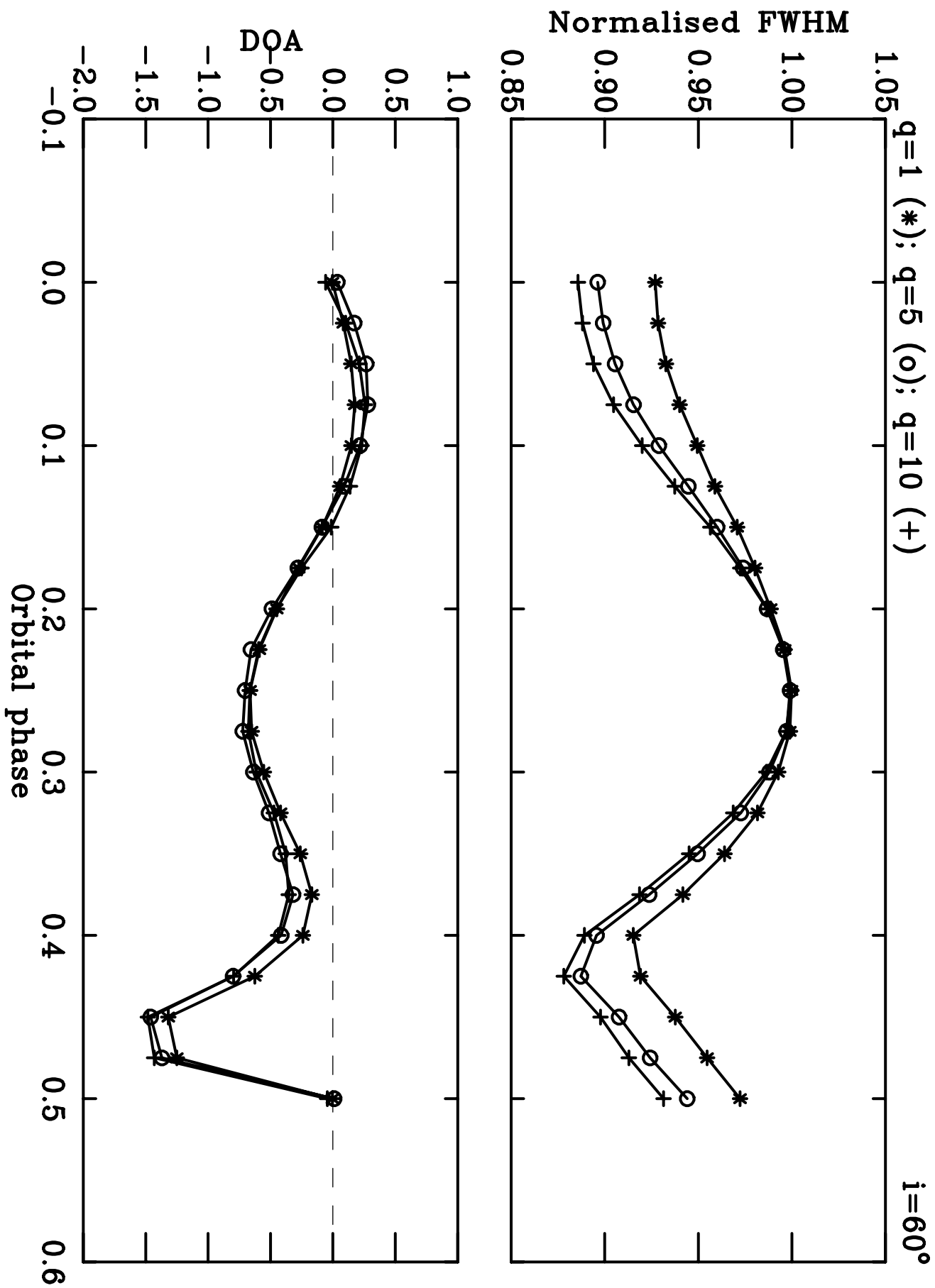


Figure 7

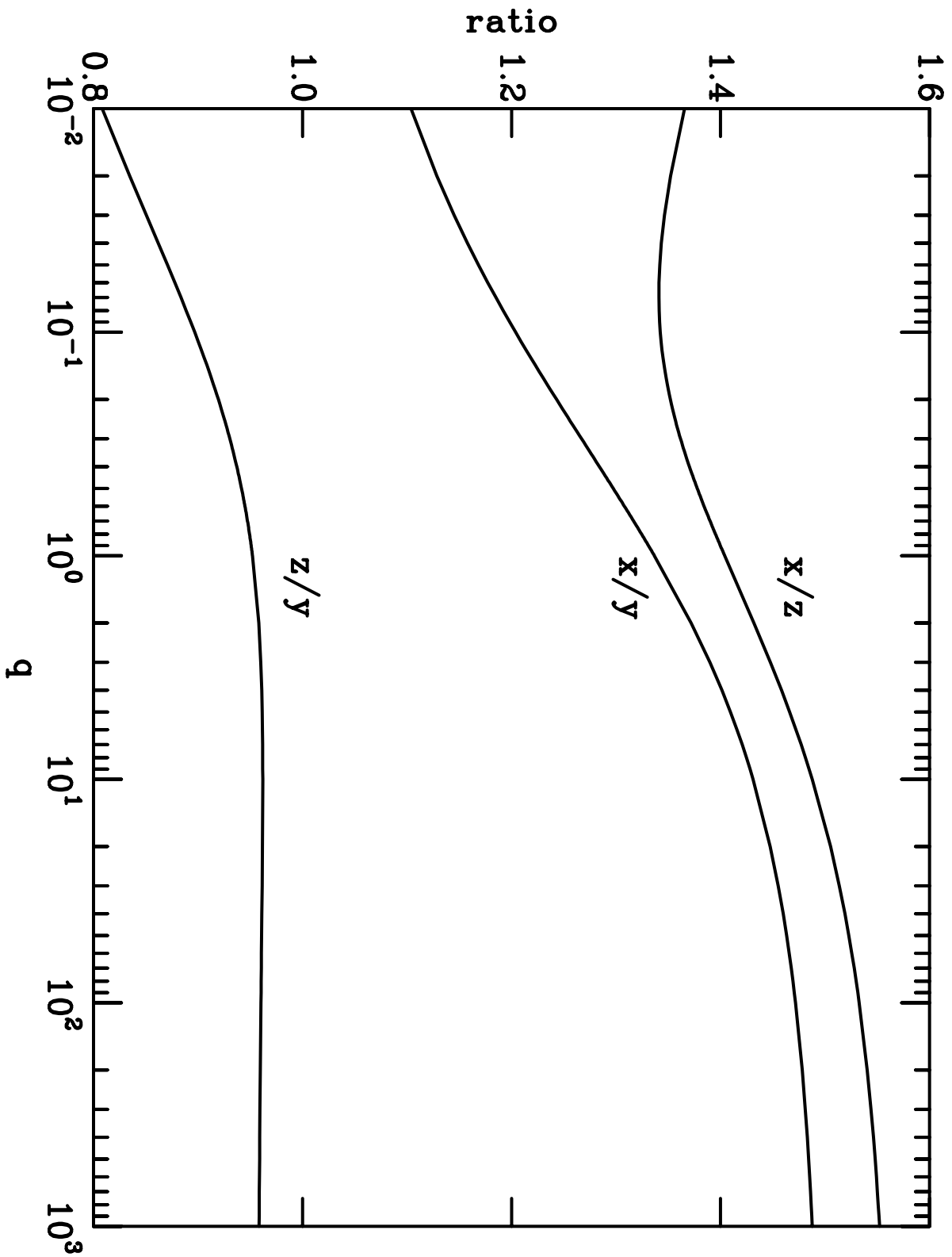


Figure 8a

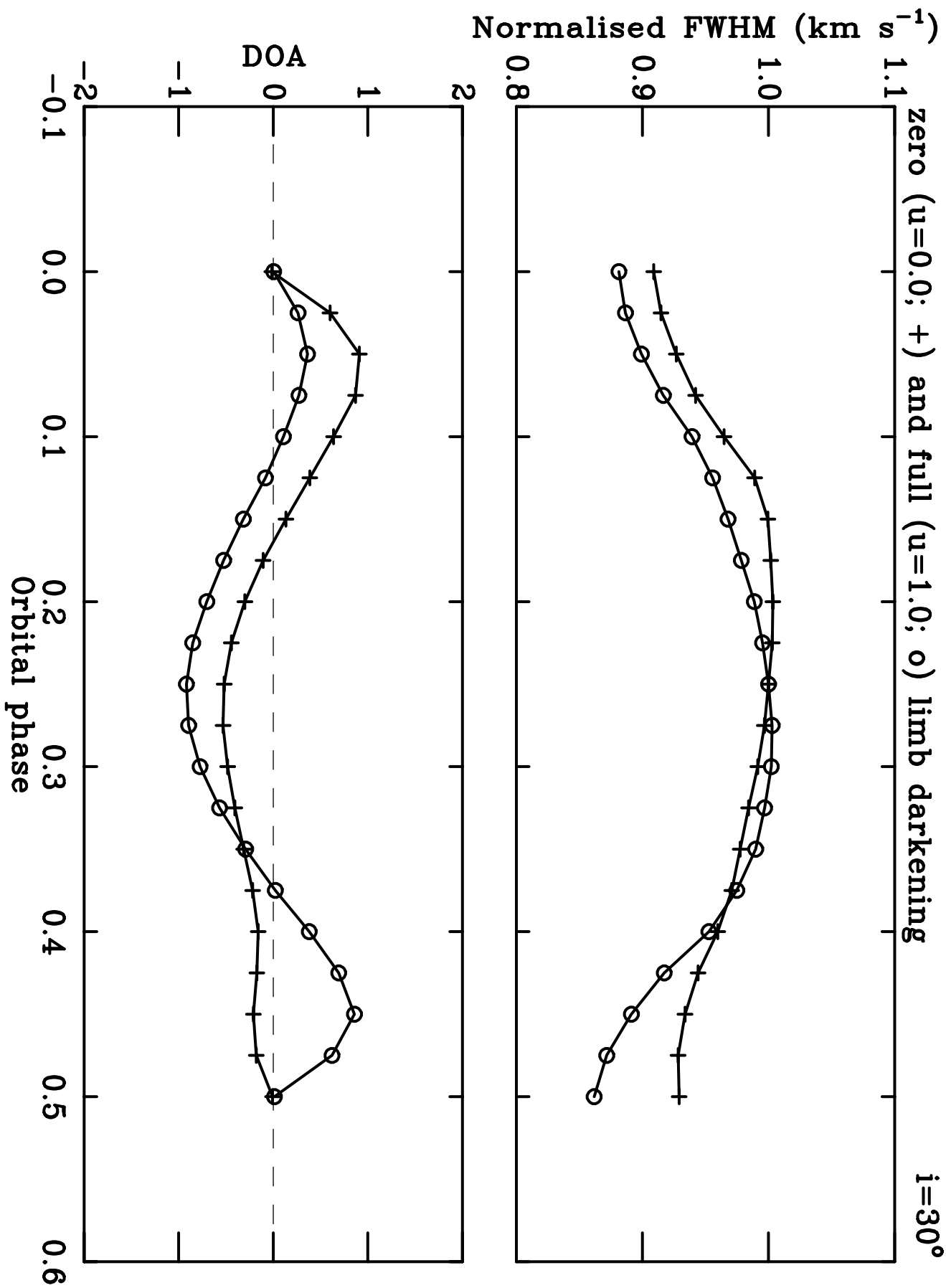


Figure 8b

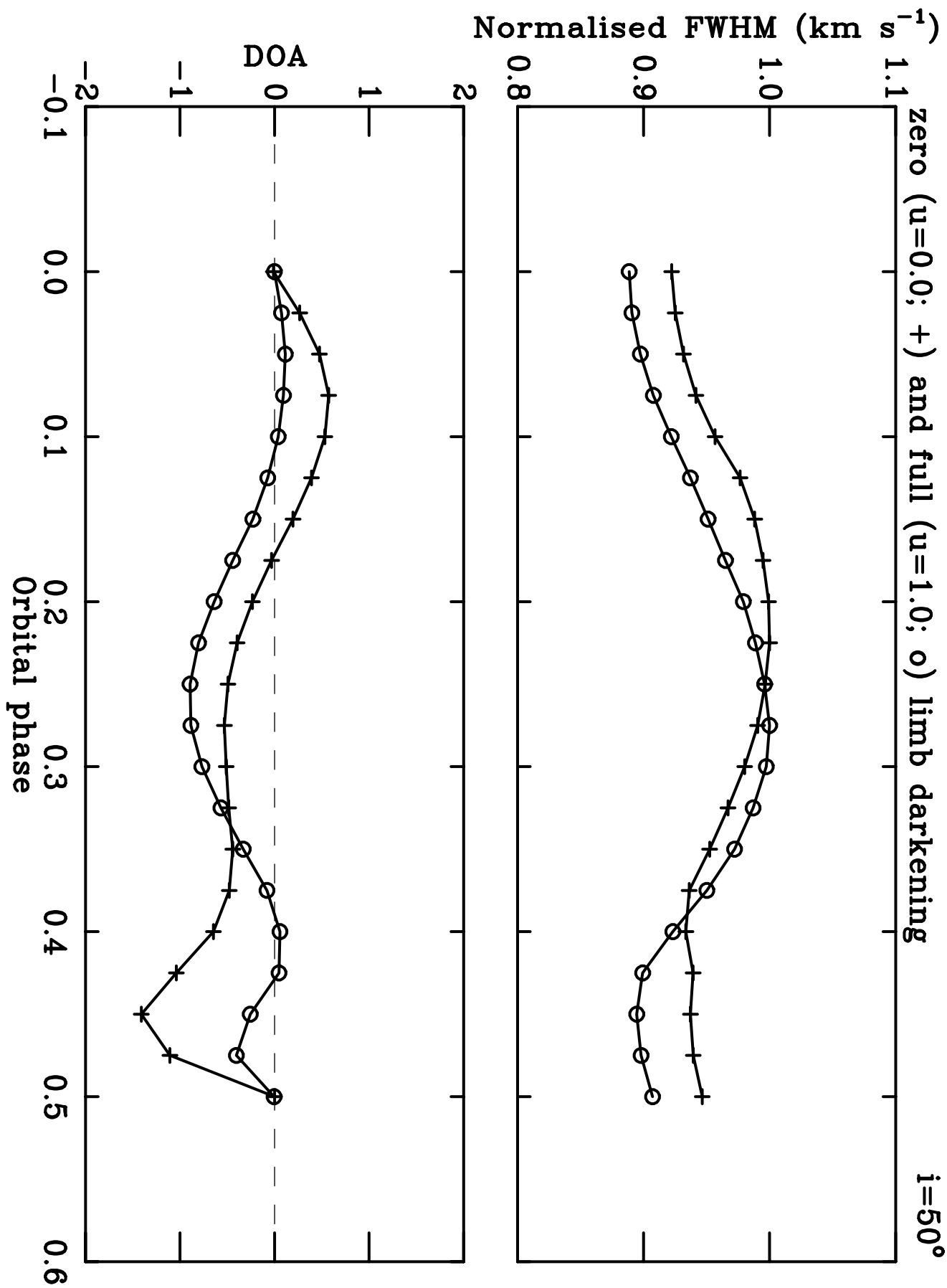


Figure 9a

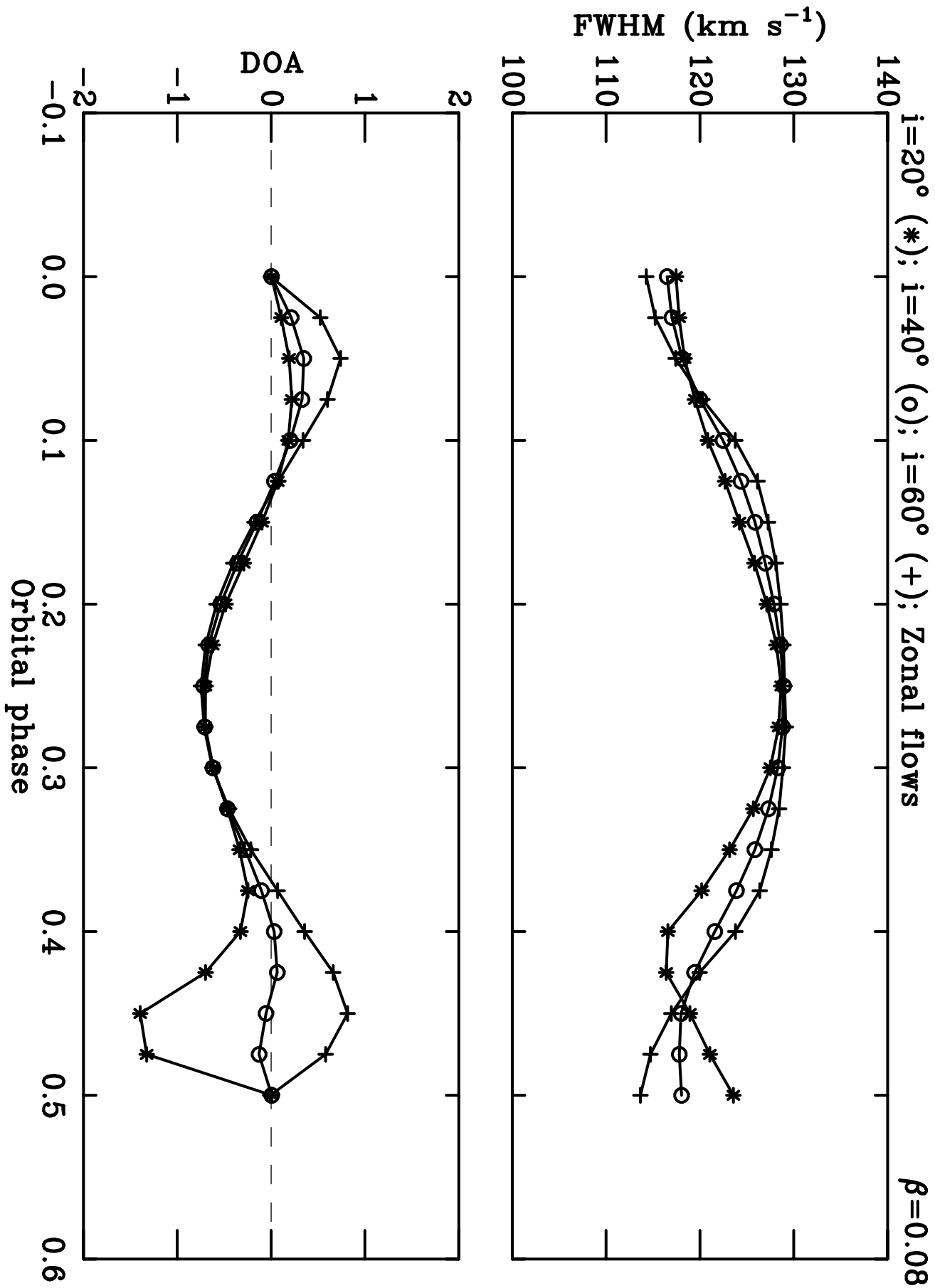


Figure 9b

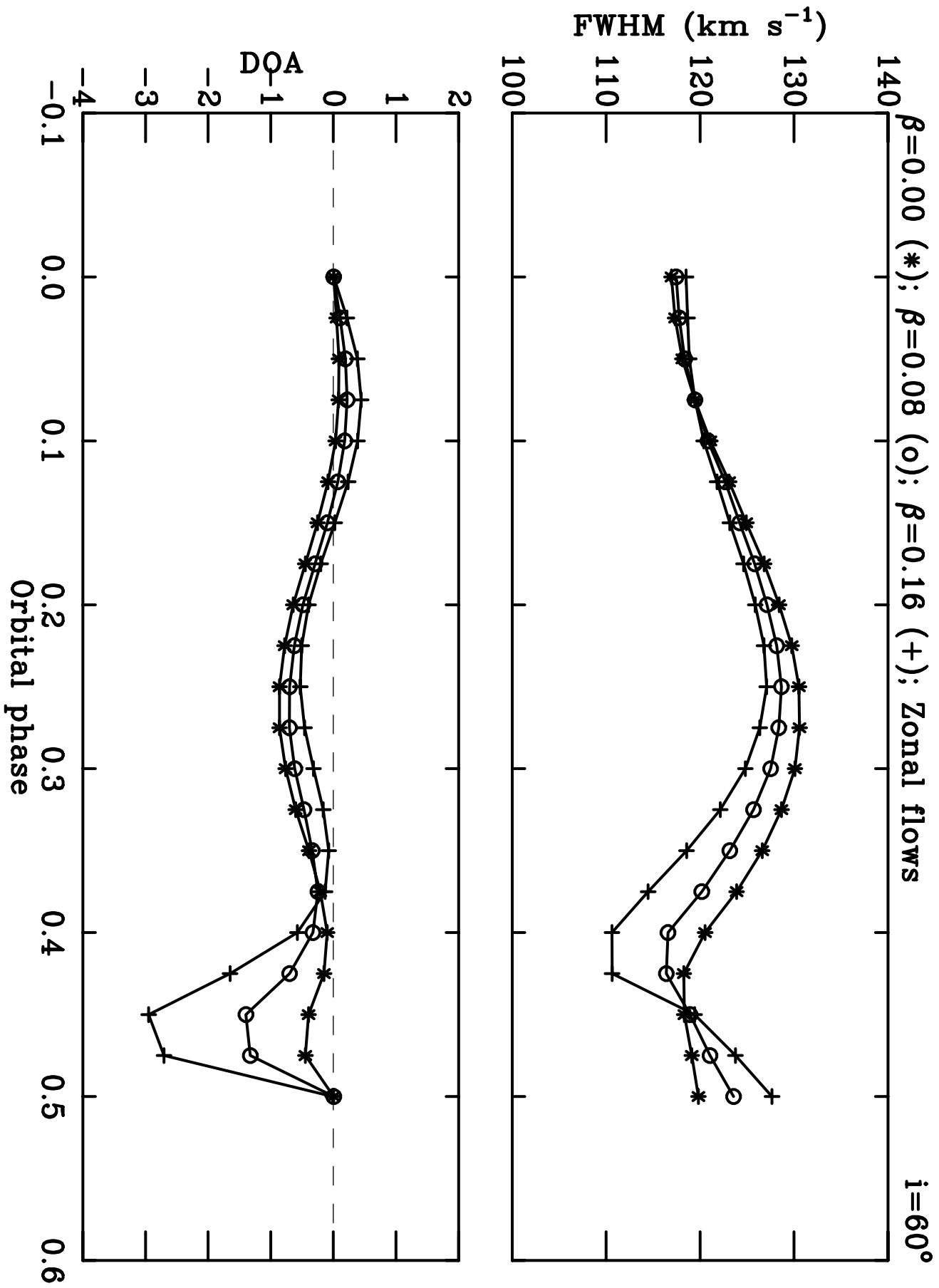


Figure 10

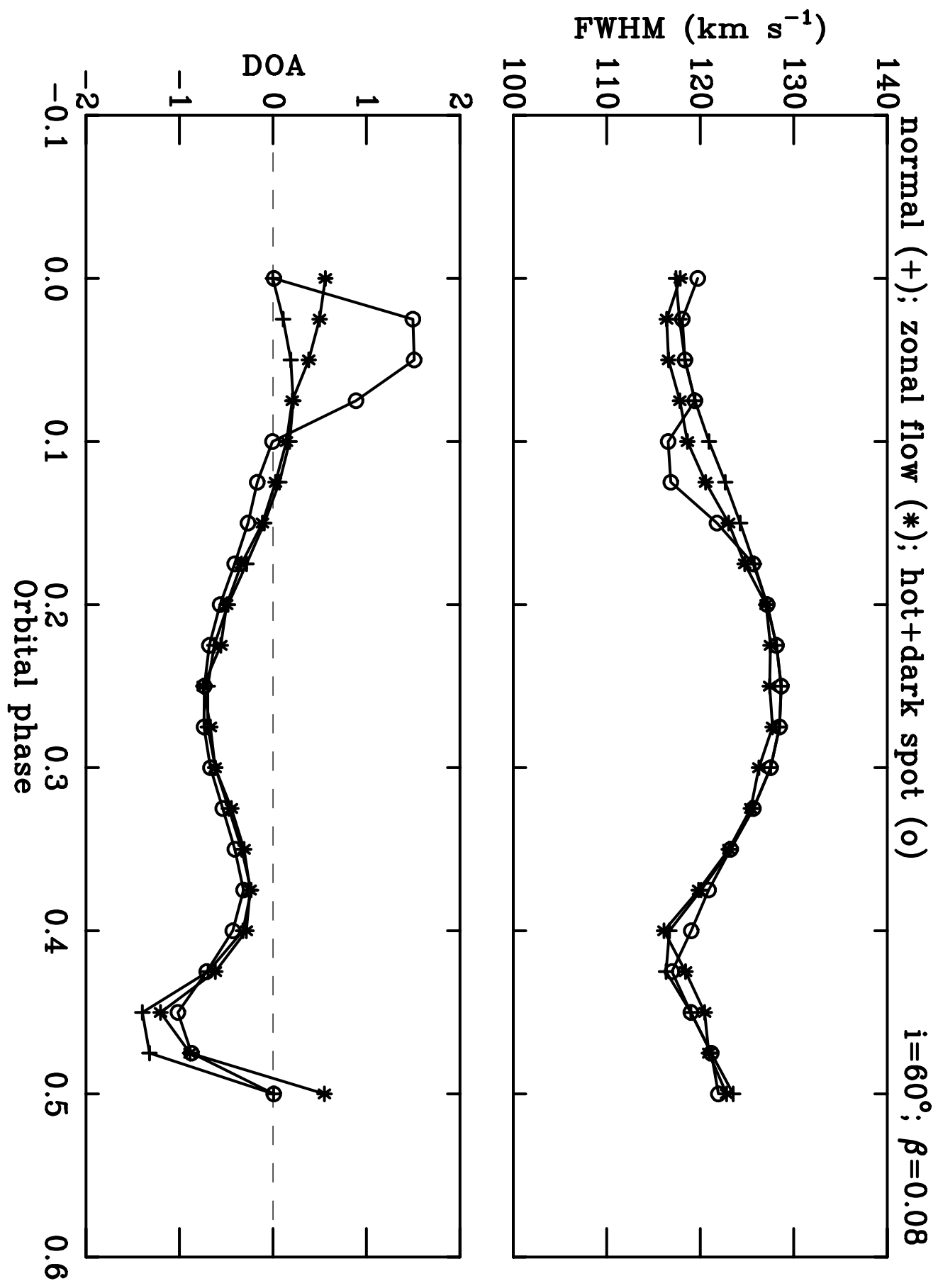


Figure 11

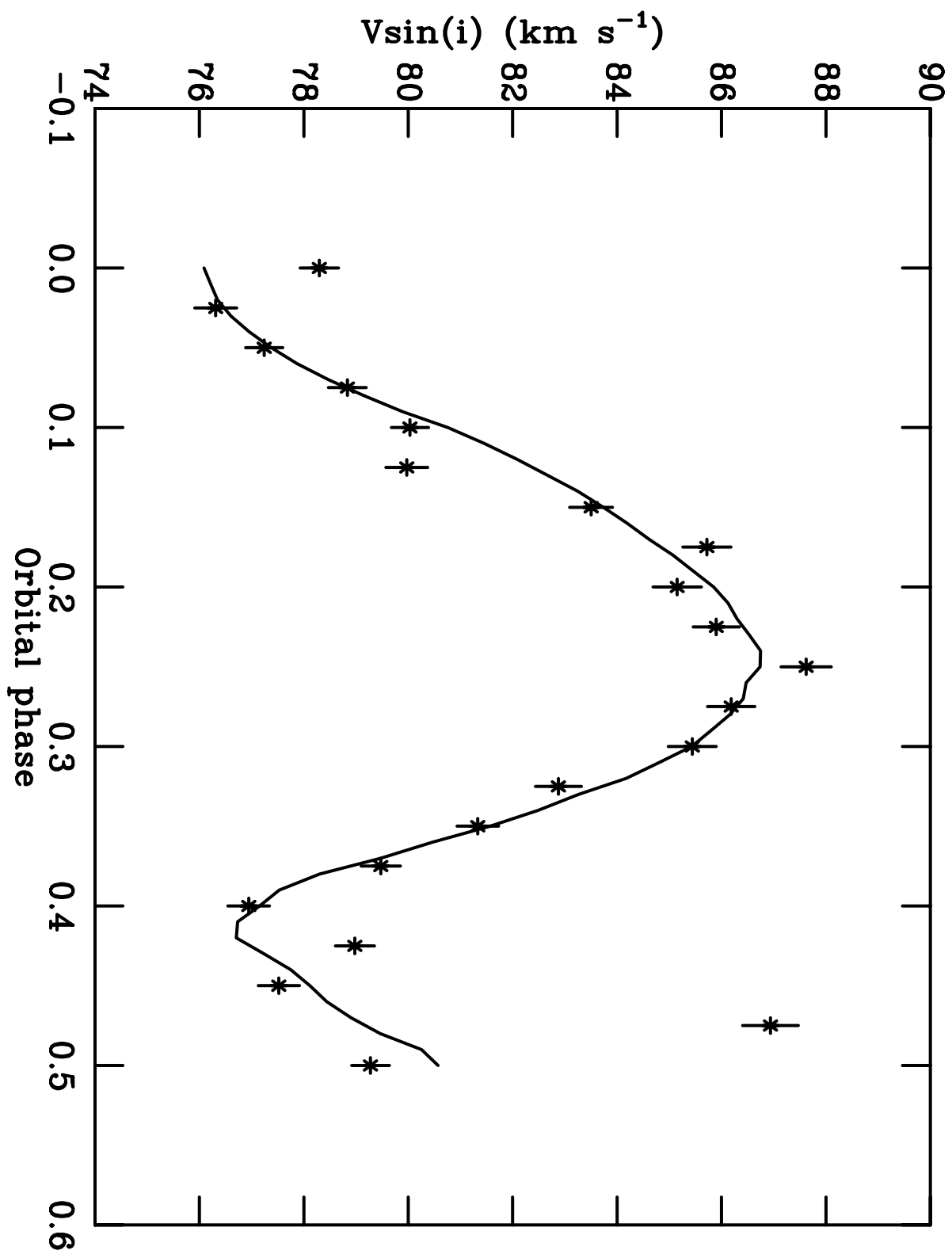


Figure 12

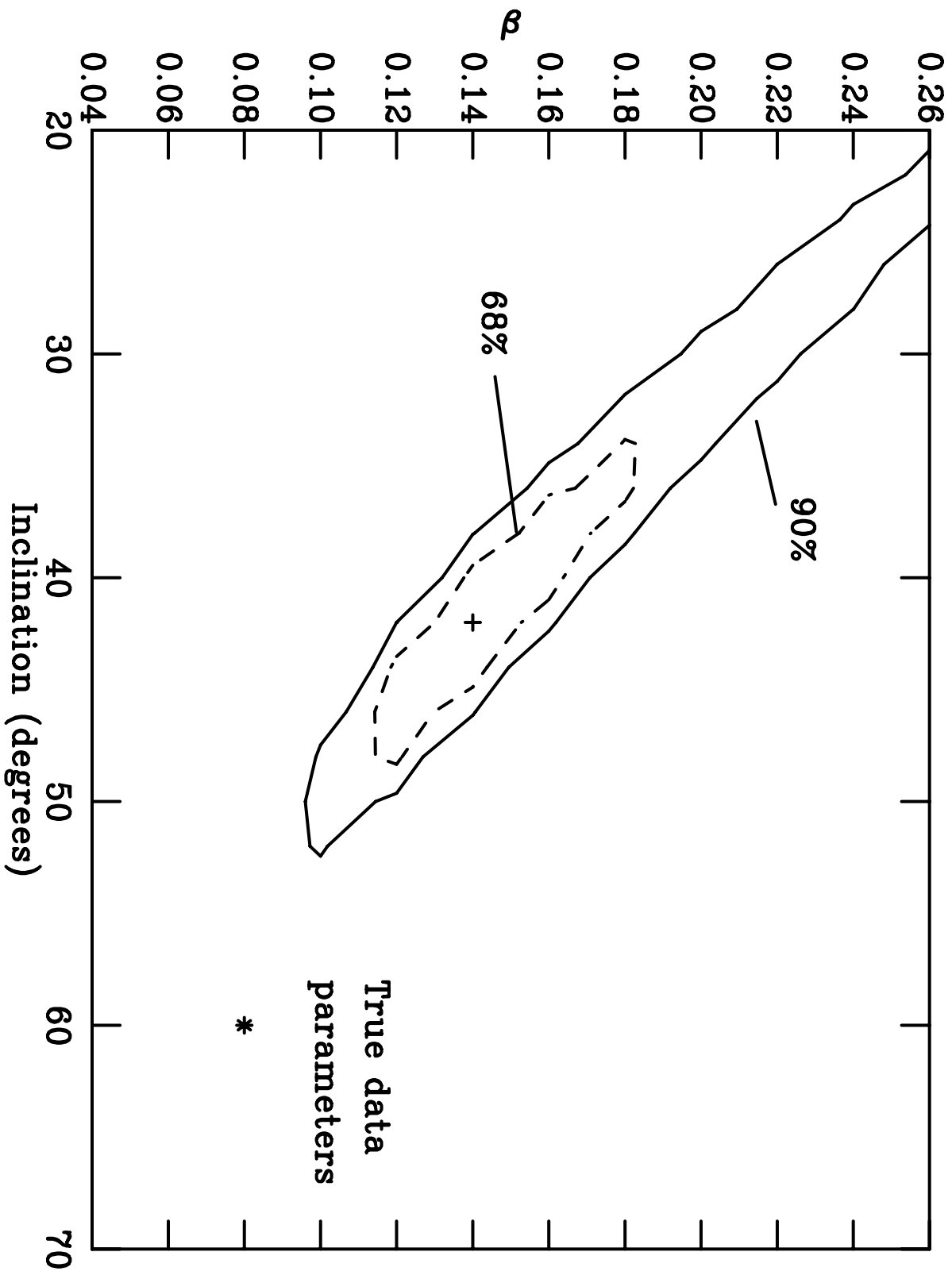


Figure 13

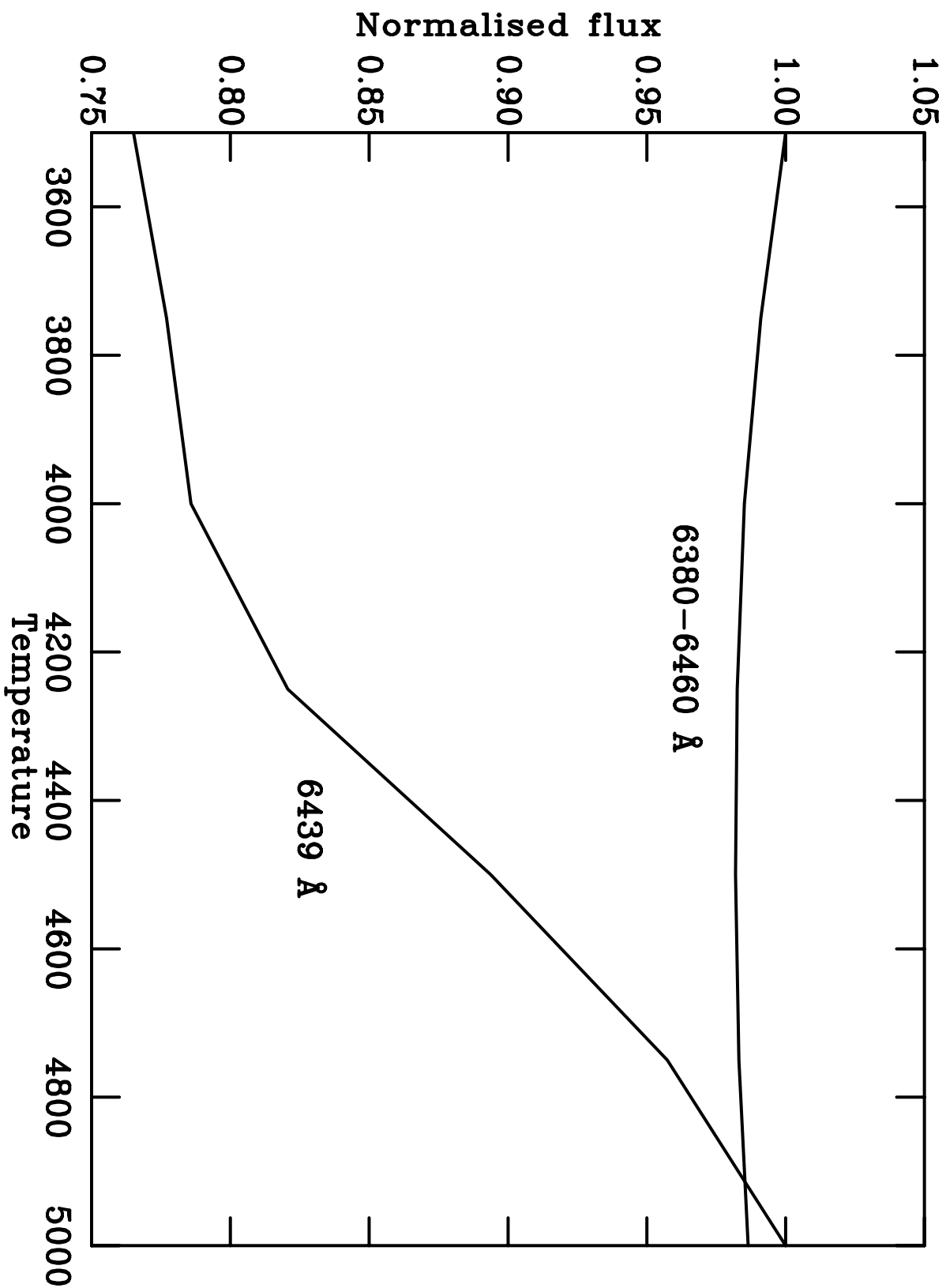


Figure 14

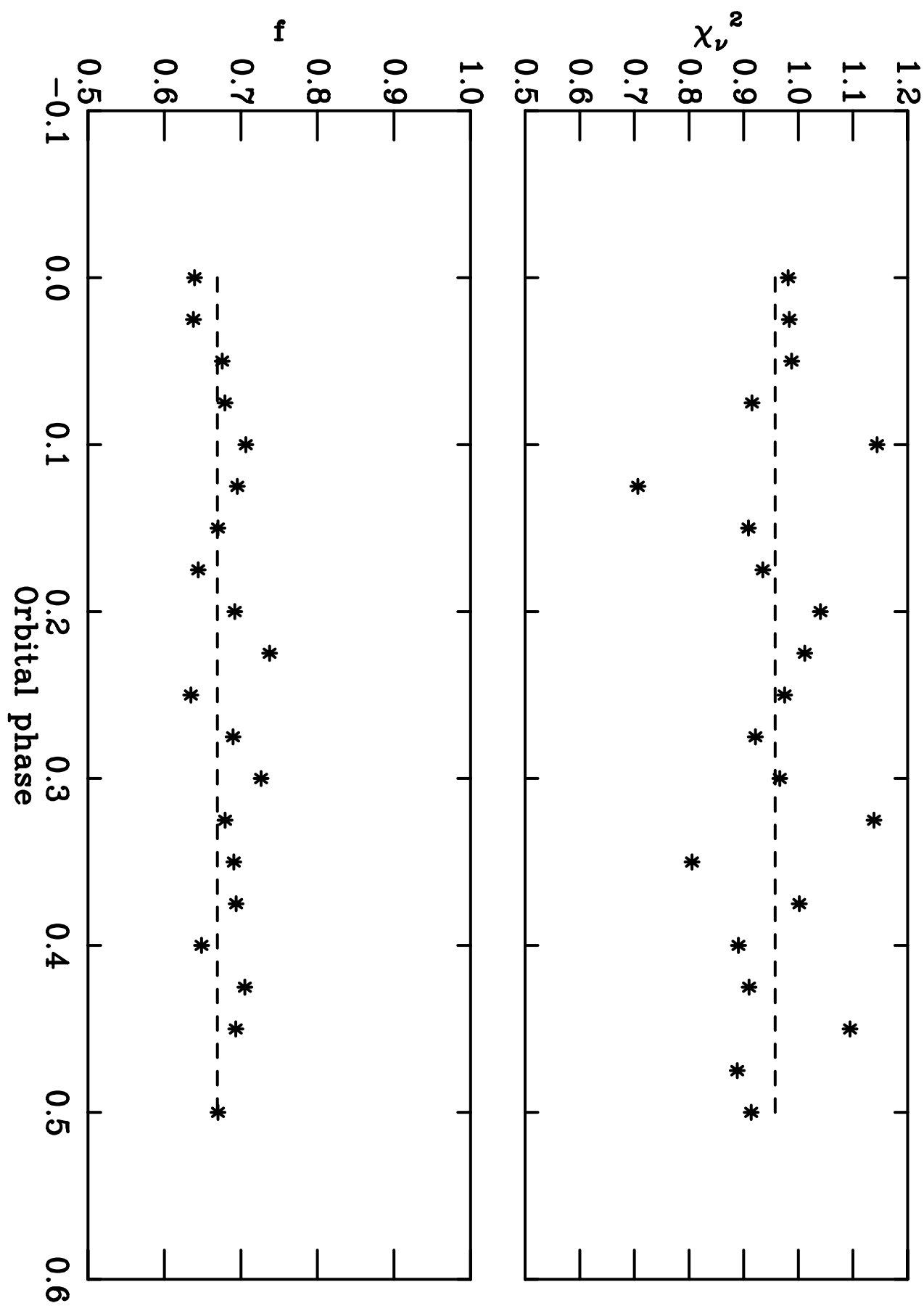


Figure 15

